Zhang et al. *Zool. Res.* 2023, 44(3): 505−521
https://doi.org/10.24272/j.issn.2095-8137.2022.440

ZR | Zoological Research

Article Open Access

Transcription factor *Dmrt1* triggers the SPRY1-NF-κB pathway to maintain testicular immune homeostasis and male fertility

Meng-Fei Zhang[1], Shi-Cheng Wan[1], Wen-Bo Chen[1], Dong-Hui Yang[1], Wen-Qing Liu[1,2], Ba-Lun Li[1], Aili Aierken[1], Xiao-Min Du[1], Yun-Xiang Li[1], Wen-Ping Wu[1], Xin-Chun Yang[1], Yu-Dong Wei[1], Na Li[1], Sha Peng[1], Xue-Ling Li[3], Guang-Peng Li[3], Jin-Lian Hua[1,4,*]

[1] *College of Veterinary Medicine*, *Shaanxi Centre of Stem Cells Engineering & Technology*, *Northwest A&F University*, *Yangling, Shaanxi 712100, China*

[2] *Center of Reproductive Medicine*, *Amsterdam Research Institute Reproduction and Development*, *Academic Medical Center*, *University of Amsterdam* 1105*AZ*, *Amsterdam*, *Netherlands*

[3] *Key Laboratory for Mammalian Reproductive Biology and Biotechnology*, *Ministry of Education*, *Inner Mongolia University*, *Hohhot*, *Inner Mongolia* 010021, *China*

[4] *Key Laboratory of Livestock Biology*, *Northwest A&F University*, *Yangling*, *Shaanxi 712100*, *China*

ABSTRACT

Bacterial or viral infections, such as *Brucella*, mumps virus, herpes simplex virus, and Zika virus, destroy immune homeostasis of the testes, leading to spermatogenesis disorder and infertility. Of note, recent research shows that SARS-CoV-2 can infect male gonads and destroy Sertoli and Leydig cells, leading to male reproductive dysfunction. Due to the many side effects associated with antibiotic therapy, finding alternative treatments for inflammatory injury remains critical. Here, we found that *Dmrt1* plays an important role in regulating testicular immune homeostasis. Knockdown of *Dmrt1* in male mice inhibited spermatogenesis with a broad inflammatory response in seminiferous tubules and led to the loss of spermatogenic epithelial cells. Chromatin immunoprecipitation sequencing (ChIP-seq) and RNA sequencing (RNA-seq) revealed that *Dmrt1* positively regulated the expression of *Spry1*, an inhibitory protein of the receptor tyrosine kinase (RTK) signaling pathway. Furthermore, immunoprecipitation-mass spectrometry (IP-MS) and co-immunoprecipitation (Co-IP) analysis indicated that SPRY1 binds to nuclear factor kappa B1 (NF-κB1) to prevent nuclear translocation of p65, inhibit activation of NF-κB signaling, prevent excessive inflammatory reaction in the testis, and protect the integrity of the blood-testis barrier. In view of this newly identified *Dmrt1*-*Spry1*-NF-κB axis mechanism in the regulation of testicular immune homeostasis, our study opens new avenues for the prevention and treatment of male reproductive diseases in humans and livestock.

Keywords: *Dmrt1*; Spermatogenesis; Orchitis; *Spry1*; NF-κB

INTRODUCTION

The global declines in sperm quality and male infertility are of considerable concern. Approximately 15% of male infertility is caused by reproductive tract infection and inflammation (Fijak et al., 2018; Punab et al., 2017). Uropathogenic *Escherichia coli* (UPEC) strains are considered the main pathogenic cause of urogenital infection, with isolation from urine and semen samples in 50% to 95% of patients (Lu et al., 2013; Virtanen et al., 2017; Wiles et al., 2008). Bacterial or viral infection, such as from *Brucella*, mumps virus (MUV) (Wu et al., 2019, 2021a), cytomegalovirus, herpes simplex virus (Malolina et al., 2014), and Zika virus, can lead to serious reproductive disorders (Ma et al., 2016; Meinhardt, 2017). Zika virus preferentially infects Sertoli cells (SCs) in the testis, resulting in cell death and seminiferous tubule destruction (Govero et al., 2016; Hui et al., 2020). Recent evidence suggests that SARS-CoV-2 can also infect male gonads, destroy SCs and Leydig cells, and induce male reproductive dysfunction (Purpura et al., 2022; Wang & Xu, 2020). Studies have shown

Received: 11 January 2023; Accepted: 07 April 2023; Online: 10 April 2023
Foundation items: This work was supported by the National Natural Science Foundation of China (32072806, 31572399), National Key Research and Development Program of China (2022YFD1302201), Program of Shaanxi Province Science and Technology Innovation Team (2019TD-036), Major Projects of Natural Science Foundation of Inner Mongolia Autonomous Region (2020ZD10), Key Research and Development Program of Shaanxi Province (2022NY-044), and Key Technologies Demonstration of Animal Husbandry in Shaanxi Province (20221086)

*Corresponding author, E-mail: jinlianhua@nwsuaf.edu.cn

that testicular damage during infection is caused by the host immune response rather than the direct cytotoxic effects of the pathogens (Wang et al., 2018). Therefore, the study of immune regulation in inflammation-related male infertility is of great significance for clinical diagnosis and treatment.

Mammalian testes create a unique immune microenvironment called testicular immune privilege. The blood-testis barrier (BTB) consists of Sertoli-germ cell junctions, as well as Sertoli-SC junctions, which play a key role in the establishment of the testicular microenvironment to maintain full spermatogenesis (Wu et al., 2019). As the basis of the BTB, close junctions between adjacent SCs block contact between immune and spermatogenic cells, thereby creating immune tolerance (Meng et al., 2011). Impaired tight junctions in the BTB can cause orchitis (Mazaud-Guittot et al., 2010). Various cytokines and pattern recognition receptors (PRRs) expressed by SCs, such as tumor necrosis factor receptor (TNFR) and toll-like receptors (TLRs), also form part of the testicular immune microenvironment (Mruk & Cheng, 2015; Zhang et al., 2013). Under physiological conditions, low levels of proinflammatory cytokines are essential for normal spermatogenesis by regulating spermatocytes from the base of seminiferous tubules to the chamber (Lie et al., 2011; Xia et al., 2009). However, under inflammatory conditions, these cytokines are overexpressed and can damage the testicular microenvironment (Li et al., 2019). Pathogenic infection can induce the innate immune response of SCs by activating TLRs, stimulating the expression of proinflammatory cytokines, including tumor necrosis factor α (TNF-α), interleukin 1β (IL-1β), IL-6, and macrophage chemoattractant protein 1 (MCP-1) (Vijay, 2018; Zhang et al., 2013). High levels of TNF-α can inhibit Leydig cell testosterone production, resulting in apoptosis of male germ cells and infertility. Activation of the inflammatory response drives NF-κB-mediated gene expression to further amplify inflammation. Notably, dysregulation of NF-κB activation is linked with chronic inflammatory, infectious, and autoimmune disorders as well as cancer (Hou et al., 2021). However, the underlying regulatory mechanism of NF-κB in these diseases remains largely unknown.

The transcription factor DMRT1 contains a DNA-binding region called the DM domain, which is the most conserved domain in vertebrates and invertebrates and is involved in male sex determination (Feng et al., 2021; Ogita et al., 2020; Wang et al., 2022), functioning in somatic-cell masculinization and germ-cell development in mammals (Mawaribuchi et al., 2017). In birds, primary sex determination depends on DMRT1 dosage levels (Ioannidis et al., 2021). In adult male animals, *Dmrt1* is only expressed in SCs and undifferentiated spermatogonial stem cells (SSCs) (Lindeman et al., 2021). DMRT1 can modify chromatin status and recruit SOX9 to bind to key genomic sites, thereby regulating the formation and maintenance of SCs in mice (Lindeman et al., 2021). Recent research has shown that SCs can be reprogrammed into granulosa cells after *Dmrt1* deletion, and overexpression of *Dmrt1* in granulosa cells can reprogram granulosa cells into Sertoli-like cells (Matson et al., 2011; Minkina et al., 2014). In addition, *Dmrt1* is associated with the maintenance of SSCs in adult testes. Knockout of *Dmrt1* leads to the gradual loss of germ cells (Takashima et al., 2013; Wei et al., 2018). *Dmrt1* controls the transition of mitosis to meiosis in male germ cells by inhibiting the retinoic acid (RA) response and *Stra8* transcription (Matson et al., 2010). In early testicular development after birth, *Dmrt1* promotes the migration of pro-spermatogonia from the seminiferous tubule center to the peripheral stem-cell niche and the final differentiation to SSCs in mice (Tan et al., 2021).

We previously identified a new role of *Dmrt1* in controlling testicular innate immune response to resist pathogenic invasion and improve spermatogenesis (Wei et al., 2018, 2021). *Dmrt1* also regulates the immune response by inhibiting TLR4 signaling in goat male germline stem cells (Wei et al., 2021; Yu et al., 2021). However, the specific regulatory mechanism of *Dmrt1* for testicular inflammation remains unclear. In this study, we identified *Dmrt1* as a key regulator in the maintenance of testicular immune homeostasis. *Dmrt1*-deficient mice exhibited reduced spermatogenesis with a widespread inflammatory reaction in seminiferous tubules. Chromatin immunoprecipitation sequencing (ChIP-seq) and RNA sequencing (RNA-seq) showed that *Dmrt1* directly regulated many genes relevant to inflammatory pathways. Knockdown (KD) of *Dmrt1* or *Spry1* in the testes led to more severe inflammatory response, BTB damage, and NF-κB signaling upon treatment with lipopolysaccharide (LPS). *Spry1*, which belongs to the Sprouty gene family, is a negative regulator of receptor tyrosine kinase (RTK) signal transduction (Cabrita & Christofori, 2008) and is involved in the regulation of many diseases. *Spry1* down-regulates epidermal growth factor receptor-extracellular regulated protein kinase (EGFR-ERK) signaling and induces epithelial mesenchymal transformation (Koledova et al., 2016; Rodríguez-Mateo et al., 2017). Immunoprecipitation-mass spectrometry (IP-MS) and co-immunoprecipitation (Co-IP) experiments confirmed that SPRY1 can bind to NF-κB1 and inhibit p65 entry into the nucleus, thereby reducing NF-κB activity and inflammatory factor production. In conclusion, our data revealed an important immunomodulatory role of *Dmrt1* in the mammalian testis, which may provide a new target for the treatment of testicular inflammatory diseases.

MATERIALS AND METHODS

Animals

All animal experiments were performed in accordance with the Guide for the Care and Use of Laboratory Animals (Ministry of Science and Technology of the People's Republic of China, Policy No. 2006 398) and were approved by the Animal Care and Use Center of Northwest A&F University (Approval No. 201705A299). All male mice used in the experiments were purchased from Dashuo Laboratory Animal Limited Company (Chengdu, China). Mice were housed at room temperature (22–24 °C) on a 12-h light/12-h dark cycle with *ad libitum* access to water at the Northwest A&F University Animal Care Facility (Qin et al., 2021).

LPS administration

A single dose of LPS (Sigma L2630, USA, 10 mg/kg) was intraperitoneally injected into the male mice to induce inflammation in the testis and epididymis (Wang et al., 2021). The same volume of 1×phosphate-buffered saline (PBS) was injected as a negative control. Serum hormone levels, histopathology, TUNEL staining, immunofluorescence (IF), immunohistochemistry (IHC), and mRNA and protein levels were examined at specific time points as indicated in the respective figures.

Cell culture and cell transfection

HEK293T cells were maintained in Dulbecco's Modified Eagle

Medium (DMEM) (Corning, USA) supplemented with 10% heat-inactivated fetal bovine serum (FBS) (Gibco, USA), penicillin (Thermo Fisher Scientific, USA, 100 IU/mL), and streptomycin (Thermo Fisher Scientific, USA, 100 IU/mL) at 37 ℃ (5% CO_2) for 24 h. TM4 cells were maintained in DMEM/F12 (Corning, USA) supplemented with 5% heat-inactivated horse serum, 2.5% heat-inactivated fetal bovine serum, penicillin (100 IU/mL), and streptomycin (100 IU/mL) at 37 ℃ (5% CO_2) for 24 h. Primary SCs from the testes were maintained in DMEM/F12 with 10% heat-inactivated fetal bovine serum, penicillin (100 IU/mL), and streptomycin (100 IU/mL) at 37 ℃ (5% CO_2) for 24 h. Cell transfection was performed using Lipo6000 Transfection Reagent (Beyotime, China, C0526) according to the manufacturer's instructions. The small interfering RNA (siRNA) sequences are listed in Supplementary Table S1.

Generation of *Dmrt1* and *Spry1* KD mice

Lentivirus production was conducted as described previously (Zhang et al., 2021). Assistant plasmids PAX2 and VSVG were co-transfected with U6-promoter vector in HEK293T cells. The shDmrt1 or shSpry1 lentiviruses were collected 48 h later after transfection. The primers required to construct the vector are listed in Supplementary Table S2. For *Dmrt1* or *Spry1* KD *in vivo*, we immediately delivered siRNA or interfering virus to the testis, as described previously (Brinster & Avarbock, 1994; Kanatsu-Shinohara et al., 2016). For seminiferous tubule transplantation (STT), approximately 100 μL of interfering virus or siRNA suspension was injected through the efferent duct into the left or right testis of normal mice, respectively. The testes injected with vector virus were used as the control group. The seminiferous tubule injection protocol was conducted following previous research (Kanatsu-Shinohara et al., 2003; Ogawa et al., 1997). The testes were collected for further experiments one week after injection (Goodyear & Brinster, 2017). There were at least 20 mice in each group, Si-NC: vector or negative siRNA group, Si-Dmrt1: knockdown of *Dmrt1* group, Si-Spry1: knockdown of *Spry1* group. The siRNA sequences used in the present study are listed in Supplementary Table S1.

Enzyme-linked immunosorbent assay (ELISA)

Blood samples were derived from wild-type, Si-Dmrt1, and Si-Spry1 mice, and serum was obtained by centrifugation at 2 000 r/min for 5 min at 4 ℃. Serum glial cell line-derived neurotrophic factor (GDNF) and anti-sperm antibody (AsAb) levels were measured using an ELISA Assay Kit (FANKEL, China, GDNF F2110-B, AsAb F2532-B) in accordance with the manufacturer's instructions. For the measurement of inflammatory factors (TNF-α, IL-6), equal amounts of testis tissue from wild-type, Si-Dmrt1, and Si-Spry1 mice were lysed, and inflammatory factor levels were determined using respective ELISA kits according to the manufacturer's instructions (FANKEL, China, IL-6 F2163-B, TNF-α F2132-B).

Histology, IHC, IF staining, and electron microscopy

Experimental procedures were conducted as reported previously (Du et al., 2018). For histological detection, the testis and epididymis were fixed in 4% paraformaldehyde (Sigma, USA) for 24 h and embedded in paraffin. The paraffin sections (2 μm thick) were cut with a rotary microtome, then de-waxed and stained with hematoxylin and eosin (H&E).

For IHC analysis, tissue sections were first deparaffinated and rehydrated. Antigen retrieval was performed with Tris/EDTA pH9.0 buffer (microwave to boil over for 15–20 min and cooled at room temperature). After washing with PBS, sections were treated with 3% hydrogen peroxide for 10 min, followed by 0.3% Triton X-100 for 10 min and washing with PBS three times. Sections were then blocked with 5% bovine serum albumin (BSA, Sigma, USA) in PBS for 1 h at room temperature. The primary antibody was diluted at 1:200 in 2.5% BSA-PBS according to the manufacturer's suggestion and incubated with tissue sections overnight at 4 ℃. The sections were then washed three times with PBS. The secondary antibody was diluted at 1:400 and incubated with sections for 1 h at room temperature, followed by washing with PBS three times. The sections were then stained by DAB (Beyotime, China, 1: 50) for 70 s at room temperature. After washing with PBS, the sections were stained with hematoxylin for 5 min at room temperature, followed by 1% ammonia treatment for 1 min. Images of sections were taken on an inverted microscope (Nikon, Japan).

For IF, the primary antibody was diluted from 1:100 to 1:400 in 2.5% BSA-PBS with 0.1% Triton X-100 (Sigma, USA) following the manufacturer's suggestions, and incubated with sections overnight at 4 ℃. The sections were then washed three times with PBS. The secondary antibody was diluted 1:400 and incubated for 1 h at room temperature, followed by washing with PBS three times. Hoechst was diluted 1:1 000 and stained for 20 min, followed by washing with PBS three times. Images were taken on an EVOS FL fluorescence microscope (AMG, USA) (Zhang et al., 2022).

Antibodies and reagents used in the study included: anti-DMRT1 (Santa Cruz Biotechnology, sc-377167, USA), anti-DDX4 (Abcam, ab13840, UK), anti-ZBTB16 (Bioss, bs-5971R, China), anti-SYCP3 (Abcam, ab15093, UK), anti-TNF-α (Proteintech, 60291-1-Ig, China), anti-IL-6 (Proteintech, 21865-1-AP, China), anti-p65 (Proteintech, 66535-1-Ig, China,), anti-TLR4 (Proteintech, 19811-1-AP, China), anti-SPRY1 (Immunoway, YN3905, USA), anti-Claudin 1 (Proteintech, 28674-1-AP, China), anti-ZO1 (Proteintech, 21773-1-AP, China), anti-SOX9 (Abcam, ab185230, UK), normal rabbit IgG (Sigma, 12-370, USA), normal mouse IgG (Sigma, 12-371, USA), DAPI (Beyotime, C1002, China), Alexa Fluor 488 (ZSGB-BIO, ZF-0511, China), Alexa Fluor 594 (ZSGB-BIO, ZF-0513, China), universal two-step detection kit (ZSGB-BIO, PV-9000, China), and DAB detection kit (Beyotime, P0202, China).

For electron microscopy analysis, the testes were fixed in 2.5% glutaraldehyde solution (Sigma, USA) in phosphate buffer, collected on poly-L-lysine-coated glass coverslips, post-fixed in osmium tetroxide, dehydrated through a series of ethanol gradients, and subjected to critical point drying and coating with gold/palladium. Finally, the samples were analyzed using a transmission electron microscope (Tecnai G2 Spirit Bio, FEI, USA).

TUNEL staining

Apoptosis in the testes and cells was detected by TUNEL staining following the manufacturer's protocols (Beyotime, C1090, China). Images were observed using an EVOS FL fluorescence microscope (AMG, USA), with the proportion of positive cells positively correlated with the rate of cell apoptosis (Lei et al., 2019).

RNA extraction, reverse transcription, and quantitative real-time polymerase chain reaction (qRT-PCR)

We performed qRT-PCR analysis in accordance with previous

study (Zhang et al., 2021). Total RNA was extracted from the testis, epididymis, other organs (heart, liver, spleen, lung, kidney, and brain), and different cells (including TM4 cells) using TRIzol Reagent (TaKaRa, 9108, Japan). The cDNA was synthesized using a reverse transcription kit (Thermo Fisher Scientific, USA). Analysis via qRT-PCR was conducted using SYBR qPCR Master Mix (Vazyme Biotech, Q311-02, China) on a CFX96 qPCR system (Bio-Rad, USA). The specific primer sequences are listed in Supplementary Table S3.

Western blotting, immunoblotting, and Co-IP

The western blotting protocols followed our previous study (Du et al., 2018). Testes, TM4 cells, primary SCs, and HEK293T cells were collected with NP40 lysis buffer (Beyotime, China) containing phosphatase and protease inhibitors. Proteins were collected from the cell lysates after centrifugation at 12 000 r/min for 20 min at 4 °C. After concentration determination using the Bradford assay (Tiangen Biotech, PA102, China), proteins were denatured in loading buffer, followed by separation using sodium dodecyl sulfate-polyacrylamide gel electrophoresis (SDS-PAGE), as described previously (Zhang et al., 2021). The results were detected using a Bio-Rad imaging system (Bio-Rad, USA) and quantified using ImageJ (V1.48d). Nuclear and cytoplasmic proteins were extracted using a Nuclear and Cytoplasmic Protein Extraction Kit (Beyotime, P0027, China) in accordance with the manufacturer's suggestions. Data were analyzed by immunoblotting.

For Co-IP or IP, the cells were collected and lysed in NP-40 lysis buffer (Beyotime, P0013, China) for 30 min. The lysate was centrifuged at 12 000 r/min for 10 min at 4 °C, and the supernatants were incubated with anti-Flag magnetic beads (Beyotime, P2115, China) or anti-HA magnetic beads (Beyotime, P2121, China) for 4 h at 4 °C. The resin was washed five times and eluted in 2×SDS-PAGE sample buffer. The sample was boiled and loaded on SDS-PAGE gel. Coomassie blue staining was performed following the manufacturer's instructions (Tiangen Biotech, PA101, China). The lysates were subjected to SDS-PAGE, transferred onto polyvinylidene fluoride (PVDF) membranes, and then blotted with indicated antibodies (Hou et al., 2021).

Antibodies and kits used in this study include: anti-DMRT1 (1:500, Santa Cruz Biotechnology, sc-377167, USA), anti-beta actin (1:2 000, Proteintech, 66009-1-Ig, China), anti-TNF-α (1:1 000, Proteintech, 60291-1-Ig, China), anti-IL-6 (1:1 000, Proteintech, 21865-1-AP, China), anti-IL-1β (1:1 000, Proteintech, 16806-1-AP, China), anti-NF-κB p65 (1:1 000, CST, #8242, USA), anti-phospho-NF-κB p65 (1:1 000, CST, #3033, USA), cleaved Caspase3 (1:1 000, CST, #9661, USA), anti-NF-κB1 (1:1 000, Proteintech, 14220-1-AP, China), anti-NF-κB2 (1:1 000, Proteintech, 10409-2-AP, China), anti-SPRY1 (1:2 000,, Immunoway, YN3905, USA), anti-FLAG-Tag (1:1 000, Sigma, F1804, USA), anti-HA-Tag (1:1 000, Santa Cruz Biotechnology, sc-7392, USA), anti-PCNA (1:1 000, Proteintech, 24036-1-AP, China), anti-mouse IgG-HRP (1:3 000, Boster, BA1050, USA), anti-rabbit IgG-HRP (1:3 000, Boster, BA1054, USA), and CBB Fast Staining Solution (Tiangen Biotech, PA101, China). Band intensities from three independent experiments were determined by densitometry using ImageJ and significant differences were determined using Student's *t*-test. Uncropped original western blots are provided in the Supplementary Materials.

Vector construction and bimolecular fluorescence complementarity (BiFC)

Truncated SPRY1 expression constructs with N-terminus (aa1–180) and C-terminus (aa181–313) were generated by PCR amplification using mouse testis cDNA. These fragments were inserted into VN173-FLAG or VC155-HA to synthesize recombinant proteins (Yin et al., 2021). Each required tagged protein expression construct was transfected in HEK293T cells with Lipo6000 (Beyotime, C0526, China) according to the manufacturer's protocols. The green fluorescent protein (GFP) of cells was observed and recorded using a fluorescence microscope (AMG, USA) 48 h after transfection. Finally, the cells were collected, followed by Co-IP with anti-FLAG and anti-HA antibodies.

Dual-luciferase reporter assay

The luciferase reporter plasmids pGL3-Basic, pGL3-Spry1, and pCDH-Dmrt1 were stored at the Shaanxi Centre of Stem Cells Engineering & Technology, Northwest A&F University. The vectors were constructed by cloning the promoter of *Spry1* into the pGL3-Basic plasmid (Promega, USA). A total of 50 ng of pGL3-Basic vector or pGL3-Spry1-promoter supplemented with pCDH-Dmrt1 was co-transfected into TM4 cells in a 48-well plate using transfection reagent Lipo6000, followed by incubation in Opti-MEM for 30 min at 37 °C. A dual-luciferase reporter system (Beyotime, China) was used to evaluate promoter activity (as determined by fluorescence levels) according to the manufacturer's instructions. Fluorescence levels were assessed using the BHP9504 optical analysis system (Hamamatsu Photonics, Japan) (Wei et al., 2021).

Assessment of sperm motility and sperm count

Sperm derived from wild-type mice treated with siRNA or control siRNA were collected from the cauda epididymis with a syringe and adjusted to 1×10^6 cells/mL using PBS. The sperm were incubated in medium for 15 min at 37 ℃, after which 4 μL of sperm suspension was placed in a counting chamber (0.01 mm^2, 10 μm deep) and assessed for motility characteristics at 37 °C. Sperm morphology was observed under a microscope after hematoxylin staining, and the ratio between normal and abnormal sperm was calculated for each group. Data were recorded using an inverted microscope (Nikon, Japan). For each sample, 10 randomly selected fields were examined (Wang et al., 2021).

RNA-seq and data analysis

To assess molecular regulation of *Dmrt1* and *Spry1* in mouse testes *in vivo*, Si-NC and Si-Dmrt1-injected testes with two biological replicates were subjected to transcriptome sequencing by Wuhan Seqhealth Technology (China). Total RNA was extracted from the testes using TRIzol Reagent (Invitrogen, cat. NO 15596026, USA) following the methods provided with the product instructions. RNA quantity was measured by spectrophotometry analysis and quality was verified by agarose gel electrophoresis (Yang et al., 2022). DNA digestion was carried out after RNA extraction using DNaseI. RNA quality was determined by A260/A280 using a NanoDrop™ One Spectrophotometer (Thermo Fisher Scientific, USA). RNA integrity was confirmed by 1.5% agarose gel electrophoresis. Qualified RNA was finally quantified by Qubit v3.0 using a Qubit™ RNA Broad Range Assay Kit (Life Technologies, Q10210, USA).

Total RNA (2 μg) was used for stranded RNA-seq library

preparation using a KC-Digital™ Stranded mRNA Library Prep Kit for Illumina® (Catalog NO. DR08502, Wuhan Seqhealth Technology, China) following the manufacturer's instructions. The kit eliminates duplication bias in PCR and sequencing steps by using unique molecular identifiers (UMIs) of eight random bases to label pre-amplified cDNA molecules. Library products corresponding to 200–500 bp were enriched, quantified, and sequenced on a NovaSeq 6000 sequencer (Illumina, USA) with the PE150 model.

Raw sequencing data were first filtered using Trimmomatic (v0.36), with low-quality reads discarded and reads contaminated with adaptor sequences trimmed. Clean reads were further treated with in-house scripts to eliminate duplication bias introduced in library preparation and sequencing. In brief, clean reads were first clustered according to the UMI sequences, in which reads with the same UMI sequence were grouped into the same cluster. Reads in the same cluster were compared to each other by pairwise alignment and reads with sequence identity over 95% were then extracted to a new sub-cluster. After all sub-clusters were generated, multiple sequence alignments were performed to obtain one consensus sequence for each sub-cluster. After these steps, any errors and biases introduced by PCR amplification or sequencing were eliminated.

The de-duplicated consensus sequences were used for standard RNA-seq analysis. They were mapped to the *Mus musculus* mm10 reference genome (ftp://ftp.ensembl.org/pub/release-88/fasta/mus_musculus/dna/Mus_musculus.GRCm38.dna.toplevel.fa.gz) using STAR software (v2.5.3a) with default parameters (Kim et al., 2013). Reads mapped to the exon regions of each gene were counted by featureCounts (Subread-1.5.1; Bioconductor), with reads per kilobase per million reads (RPKM) then calculated (Liao et al., 2014). Differentially expressed genes (DEGs) between groups were identified using the edgeR package (v3.12.1). A *P*-value cutoff of 0.05 and fold-change cutoff of 2 were used to judge statistical significance of differences in gene expression using the DESeq R package. Gene Ontology (GO) and Kyoto Encyclopedia of Genes and Genomes (KEGG) enrichment analyses of DEGs were implemented in KOBAS (v2.1.1), with a *P*-value cutoff of 0.05 to judge statistically significant enrichment (Wu et al., 2021b).

ChIP-seq and data analysis

Primary SCs (1×10^7) infected with a lentiviral vector expressing FLAG-tagged *Dmrt1* were cross-linked with 1% formaldehyde for 10 min at room temperature, after which 0.125 mol/L glycine was added, and the mixture was rested for 5 min to terminate the cross-linking reaction. The cells were then treated with cell lysis buffer and nuclei were collected by centrifugation at 2 000 ×*g* for 5 min at 4 ℃. Nuclei were treated with nucleus lysis buffer and sonicated to fragment chromatin DNA. For the lysis-sonicated chromatin, 10% was stored (named "Input"), 80% was used in IP reactions with specific anti-Flag magnetic beads (Beyotime, P2115, China) (named "IP"), and 10% was incubated with rabbit IgG (CST, USA) as a negative control (named "IgG") (Zhu et al., 2021). The Input DNA and IP DNA were extracted using the phenol-chloroform method (Zhu et al., 2021). High-throughput DNA sequencing libraries were prepared using a VAHTS Universal DNA Library Prep Kit for Illumina V3 (Catalog NO. ND607, Vazyme, China). The library products corresponding to 200–500 bp were enriched, quantified, and sequenced on a NovaSeq 6000 sequencer (Illumina, USA) using the PE150 model.

Raw sequencing data were first filtered by Trimmomatic (v0.36), with low-quality reads discarded and reads contaminated with adaptor sequences trimmed (Liao et al., 2014). The clean reads were mapped to the *Capra hircus* reference genome from GCF_001704415.1 (ftp://ftp.ncbi.nlm.nih.gov/genomes/all/GCF/001/704/415/GCF_001704415.1_ARS1/GCF_001704415.1_ARS1_genomic.fna.gz) using STAR software (v2.5.3a) (Dobin et al., 2013) with default parameters. RSeQC (v2.6) was used for read distribution analysis. MACS2 (v2.1.1) was used for peak calling. Bedtools (v2.25.0) was used for peak annotation and peak distribution analysis. Peak maps of reads across the genome were described using Integrative Genomics Viewer (IGV, v2.4.16) (Thorvaldsdóttir et al., 2013). Differential binding peaks were identified using python script with Fisher's test. Homer (v4.10) was used for motif analysis. GO and KEGG enrichment analyses of annotated genes were implemented in KOBAS (v2.1.1), with a corrected *P*-value cutoff of 0.05 to judge statistically significant enrichment (Wu et al., 2006).

Liquid chromatography-tandem mass spectrometry (LC-MS/MS)

To identify SPRY1 interacting proteins, three independent samples of SPRY1, NF-κB, IgG control were prepared. The IP procedure was the same as described above. Proteins were separated by 10% SDS-PAGE, and excised bands were used for mass spectrometry. Excised gel bands were cut and subjected to an in-gel trypsin digestion procedure, and peptides were analyzed by Jingjie PTM BioLabs (China) using an ion-trap mass spectrometer (Thermo Fisher Scientific, USA). The resulting MS/MS data were processed using Proteome Discoverer v1.3 (Hancock et al., 2019). Tandem mass spectra were searched against the UniProt database (https://www.uniprot.org/). Proteins immunoprecipitated with IgG were considered as background and not included, and proteins with fewer than two peptide hits were not included. The DAVID Bioinformatics Database (v6.7) was used to identify proteins within the Nuclear Part category of the GO Cellular Compartment (Lou et al., 2021).

Statistical analyses

All statistical analyses were performed using SPSS software (v20.0). Data were expressed as mean±standard deviation (*SD*). Unpaired two-tailed Student's *t*-test was used for comparison between two groups. One-way analysis of variance (ANOVA) followed by Dunnett's test was used for comparisons among multiple groups. All experiments had at least three independent biological replicates, except for RNA-seq, which was replicated twice. ChIP samples were collected from three independent biological experiments, then mixed for ChIP-seq. Here, $P<0.05$ was considered statistically significant (ns: Not significant; *: $P<0.05$; **: $P<0.01$; ***: $P<0.001$).

RESULTS

***Dmrt1* KD strongly inhibits spermatogenesis in mice**

Dmrt1 is only expressed in SCs and undifferentiated SSCs and is involved in male sex differentiation and sex maintenance (Lei et al., 2007). To explore the potential function of *Dmrt1* in spermatogenesis, we constructed a *Dmrt1*-deficiency mouse model by specifically knocking down

Dmrt1 in testicular seminiferous tubules (Figure 1A). *Dmrt1* expression at both the RNA and protein level was then detected. Results showed that *Dmrt1* was indeed knocked down in the Si-Dmrt1 mouse model (Figure 1B; Supplementary Figure S1A). The testes and epididymides were then obtained to detect the phenotype of seminiferous tubules and germ cells. Compared with the control group, testicular and epididymal weight showed a clear decrease in *Dmrt1* KD mice (Figure 1C). Histological analysis also showed that germ cells were deficient in seminiferous tubules in the Si-Dmrt1 mouse testes, with inflammatory syncytia in the lumen (Figure 1D). The number of sperm in epididymis of the Si-Dmrt1 group decreased markedly (Figure 1E, 1F). In addition, sperm motility in the Si-Dmrt1 group was reduced obviously (Figure 1G). However, sperm morphology in the two groups appeared normal compared with the control group (Figure 1H), and the proportion of abnormal sperm was not significantly different (Figure 1I), indicating that *Dmrt1* KD did not affect sperm morphology or deformity rate. IF staining showed that DMRT1-positive and DDX4-positive cells decreased significantly in the Si-Dmrt1 testes (Figure 1J). The marker proteins of SSCs (ZBTB16) and spermatocytes (SYCP3) were also down-regulated in *Dmrt1* KD testes, indicating that Si-Dmrt1 significantly reduced the number of spermatogenic cells (Supplementary Figure S1C, D). Taken together, these results demonstrate that *Dmrt1* KD significantly inhibits spermatogenesis and reduces germ cell numbers but has little effect on sperm morphology.

Identification of *Dmrt1* as a key regulator of inflammatory response

To further explore the potential genes regulated by *Dmrt1* in testes, we sequenced the transcriptome of Si-Dmrt1 testes (Figure 2A). We identified a total of 1 589 up-regulated and 2 141 down-regulated genes by sequencing enrichment, with some DEGs shown in the scatter diagram (Figure 2B). Genes related to SSCs and spermatogenesis, such as *Zbtb16*, *Ddx4*, and *Sycp3*, were significantly down-regulated, as were SC markers *Sox9* and *Dmrt1*. Interestingly, RNA-seq analysis indicated that several NF-κB targeting genes, such as *Tnfα*, *Il1β*, *Cxcl2*, and *Cxcl5*, were significantly up-regulated in the Si-Dmrt1 testes (Figure 2B; Supplementary Figure S1B). GO analysis revealed significant changes in several signaling pathways, such as immune response, cell adhesion, TNFR binding, and apoptosis (Figure 2C). KEGG enrichment

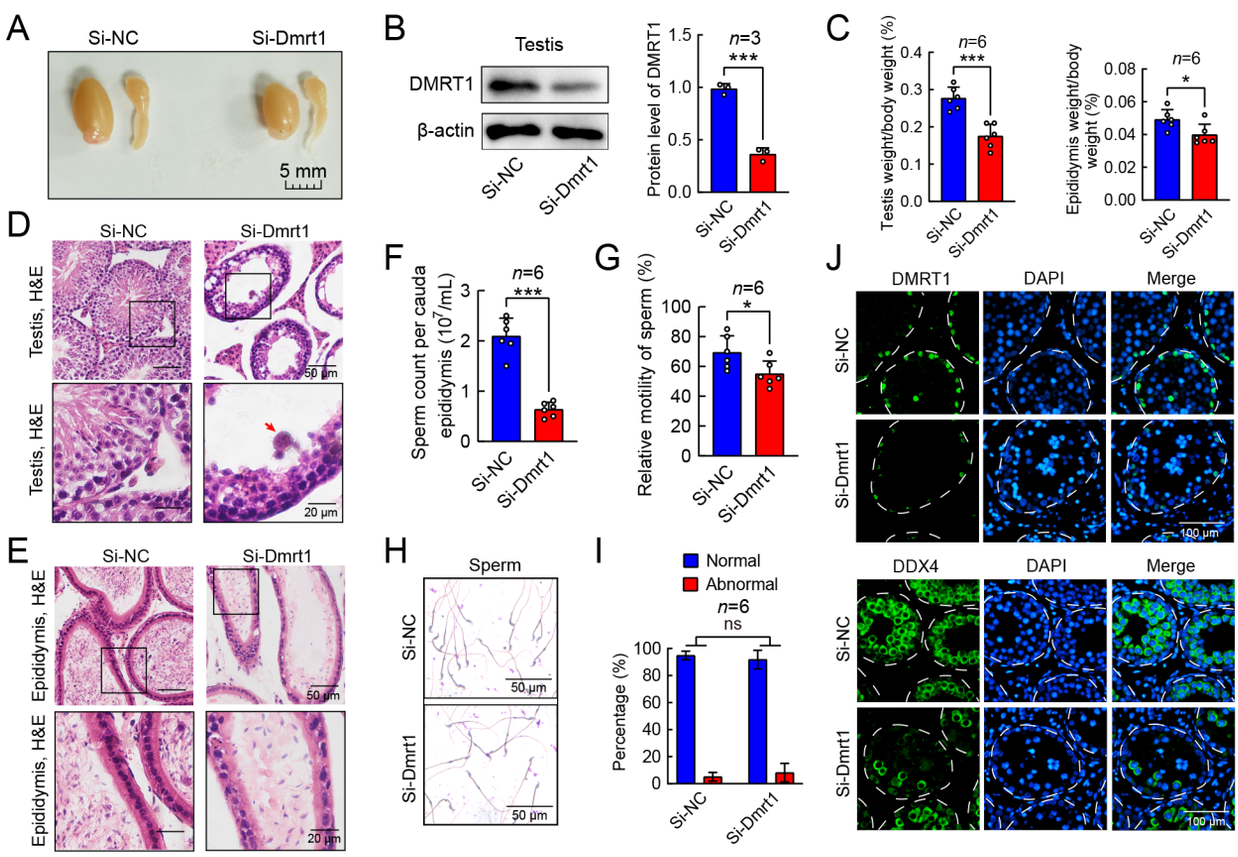

Figure 1 Targeted disruption of *Dmrt1* causes infertility and abnormal spermatogenesis in mice

A: Gross morphology of testes from Si-NC and Si-Dmrt1 mice after seminiferous tubule transplantation. Scale bar: 5 mm. B: Representative blots (left) and quantification (right) of DMRT1 protein level in testis with or without DMRT1 KD (*n*=3). Uncropped original western blots are provided in Supplementary Materials. C: Weight of testis and epididymis was markedly reduced in Si-Dmrt1 group. Data presented are ratio of testis or epididymis weight and body weight (*n*=6). D: H&E staining of testes from Si-NC and Si-Dmrt1 mice. Scale bar: 50 μm (up), 20 μm (down). Arrow indicates inflammatory syncytia in lumen. E: H&E staining of epididymis. Scale bar: 50 μm (up), 20 μm (down). F: Sperm count per cauda epididymis with or without DMRT1 KD (*n*=6). G: Relative motility of sperm with or without DMRT1 KD (*n*=6). H: Sperm morphology from Si-NC and Si-Dmrt1 mice displayed by Giemsa staining. Scale bar: 50 μm. I: Statistics of normal and abnormal sperm morphology (*n*=6). J: IF staining of DMRT1 (up) and DDX4 (down) in Si-NC and Si-Dmrt1 testes. Nuclei were stained with DAPI (blue). Scale bar: 100 μm. ns: Not significant; *: $P<0.05$; **: $P<0.01$; ***: $P<0.001$.

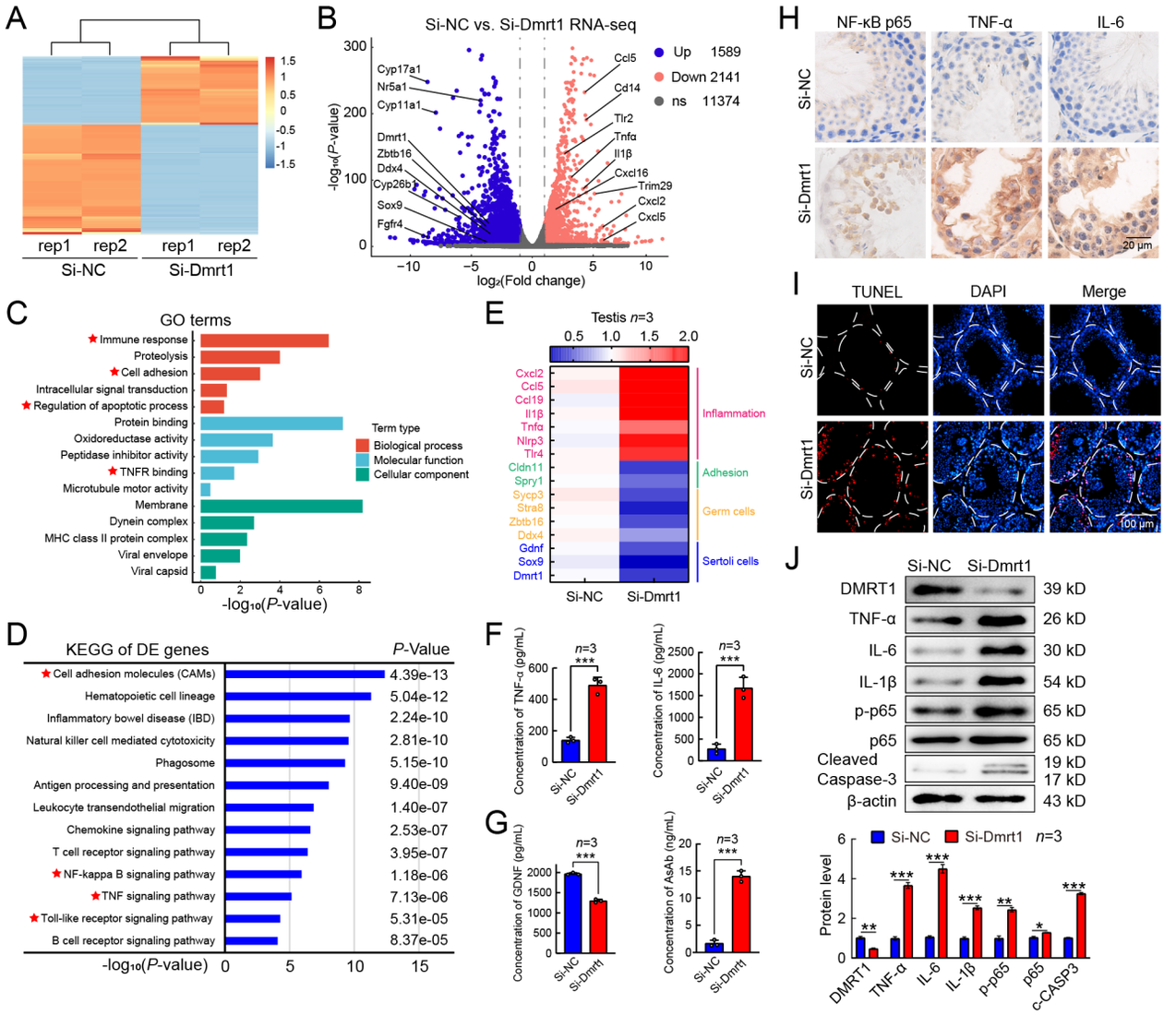

Figure 2 Identification of *Dmrt1* as a key regulator for inflammatory responses

A: Heatmap depicting gene expression patterns of Si-NC vs. Si-Dmrt1 testes. Fold-change>2 up (red) or down (blue) with $P<0.01$. B: Volcano plot of DEGs determined by RNA-seq analysis of Si-NC vs. Si-Dmrt1 testes. Dotted line represents false discovery rate (FDR) cut-off 0.01. $n=2$ biologically independent samples per condition. ns: not significant. C: Top 15 most enriched GO biological processes based on *P*-values for up-regulated and down-regulated genes in Si-NC and Si-Dmrt1 testes are shown. Red stars represent important signaling pathways focused on. D: KEGG enrichment of up-regulated and down-regulated DEGs. Red stars represent important signaling pathways focused on. E: Relative mRNA levels of inflammation- and reproduction-related genes in Si-NC and Si-Dmrt1 testes ($n=3$). F: TNF-α and IL-6 levels in testes of mice from different groups measured by ELISA ($n=3$). G: GDNF and AsAb levels in testes of mice from different groups measured by ELISA ($n=3$). H: Expression profiles of NF-κB, TNF-α, and IL-6 in testes by IHC staining. Scale bar: 20 μm. I: Cell apoptosis revealed by TUNEL staining of sections from Si-NC and Si-Dmrt1 testes. Scale bar: 100 μm. J: Representative western blots of DMRT1, TNF-α, IL-6, IL-1β, p-p65, p65, cleaved-Caspase3 (c-CASP3), and β-actin for Si-NC and Si-Dmrt1 testes. Quantitative analysis of different proteins is shown by bar graph. Data represent mean±*SD*, normalized by β-actin; $n=3$ independent experiments. ns: Not significant; *: $P<0.05$; **: $P<0.01$; ***: $P<0.001$.

analysis indicated significant changes in cell adhesion molecules and NF-κB, TNF, and TLR signaling pathways (Figure 2D). Analysis based qRT-PCR of the Si-Dmrt1 and Si-NC testes verified that while inflammation-related genes *Tnfα* and *Il1β* were significantly up-regulated in the Si-Dmrt1 groups, cell adhesion-related genes *Cldn11* and *Spry1* were significantly down-regulated, along with germ cell markers *Sycp3*, *Stra8*, *Zbtb16*, and *Ddx4* and SC markers *Gdnf*, *Sox9*, and *Dmrt1* (Figure 2E; Supplementary Figure S1A). Subsequently, ELISA analysis of mouse serum samples verified that inflammatory factors TNF-α and IL-6 were significantly higher in the Si-Dmrt1 group than in the Si-NC group (Figure 2F). In addition, the concentration of GDNF was significantly down-regulated in Si-Dmrt1 mice, indicating damage to SC function (Figure 2G). AsAb was significantly up-regulated in Si-Dmrt1 mice, indicating exposure of sperm in the seminiferous tubules to immune cells due to BTB impairment (Figure 2G). IHC staining of mouse testes verified the ELISA results, demonstrating a significant increase in the expression of NF-κB, TNF-α, and IL-6 in the Si-Dmrt1 testes (Figure 2H), consistent with RNA-seq analysis (Figure 2B). TUNEL staining further revealed that after *Dmrt1* KD, SCs and spermatogenic cells in the basement membrane of the seminiferous tubules underwent apoptosis (Figure 2I;

Supplementary Figure S1E). Additionally, the expression of p-p65 and c-Caspase3 increased significantly in Si-Dmrt1 testicular tissue (Figure 2J), indicating apoptosis as a direct cause of the decline in spermatogenic cells. Taken together, these results indicate that *Dmrt1* KD testes develop an obvious inflammatory reaction and apoptosis, with impaired BTB function and testicular immune homeostasis.

Genome-wide analysis reveals high enrichment of *Dmrt1* in gene promoters

To explore the mechanisms by which *Dmrt1* regulates testicular immune homeostasis, we performed ChIP-seq analysis of primary SCs infected with a lentiviral vector expressing FLAG-tagged *Dmrt1*, focusing on the regions of DMRT1 protein binding within 5 kb upstream and downstream of the transcription start site (TSS) and transcription end site (TES) (Figure 3A). Further analysis identified the most significant motif structures (Figure 3B). To identify genes directly targeted by *Dmrt1*, we co-analyzed the Si-Dmrt1 RNA-seq data and *Dmrt1* ChIP-seq data and identified 136 positively regulated and 86 negatively regulated genes (Figure 3C). GO and KEGG analyses of the differentially regulated genes were performed to identify the most significantly different pathways. *Dmrt1* was mainly involved in the hypoxia inducible factor 1 (HIF-1) signaling pathway, innate immune response, meiosis, adherent junction, and cell junction (Figure 3D). Visual analysis using IGV revealed high enrichment of *Dmrt1* in the promoters of target genes, leading to the activation of certain genes (e.g., *Dmrta1* (*Dmrt4*), *Spry1*, *Gata4*, *Taf4b*, and *Sox30*) or inhibition of certain genes (e.g., *Cxcl13*, *Tlr1*, and *Adamtsl1*) (Figure 3E). Taken together, ChIP-seq and RNA-seq analyses revealed that *Dmrt1* directly regulates the expression of genes involved in processes such as inflammation, meiosis, and cell adhesion, in line with its role in male spermatogenesis and newly discovered role in testicular inflammatory homeostasis.

Dmrt1* drives SC immune homeostasis through transcriptional activation of *Spry1

To further investigate target gene regulation by *Dmrt1*, we constructed SC lines by overexpressing (oeDmrt1) and knocking down *Dmrt1* (shDmrt1) (Supplementary Figure S2E). Based on qRT-PCR analysis of the OeDmrt1 and control groups (PCDH), overexpression of *Dmrt1* up-regulated the expression levels of *Spry1*, *Gata4*, *Taf4b*, and *Sox30*, and down-regulated the expression levels of *Adamtsl1*, *Tlr1*, and *Cxcl13* (Figure 4A). In contrast, qRT-PCR analysis of shDmrt1 and control cells (U6) showed that KD of *Dmrt1* down-regulated the expression levels of *Spry1*, *Gata4*, *Taf4b*, and *Sox30*, and up-regulated the expression levels of *Adamtsl1*, *Tlr1*, and *Cxcl13* (Figure 4B). These *in vitro* results validated the function of *Dmrt1* indicated by the Si-Dmrt1 testis RNA-seq and ChIP-seq data. *Spry1* is an important negative regulator of RTK signaling and participates in cell morphology, movement, and inflammatory response (Liu et al., 2021). To further explore the direct regulation of *Spry1* by *Dmrt1*, we cloned 1 000 bp *Spry1* promoter DNA into a dual-luciferase vector (*Spry1* promoter-Luc), and overexpressed *Dmrt1* and *Spry1* promoter-Luc in TM4 cells. Overexpression of *Dmrt1* stimulated the *Spry1* promoter, as indicated by the increase in luciferase activity (Figure 4C). Next, we transfected different quantities of *Dmrt1* plasmids into SCs and found that *Spry1*

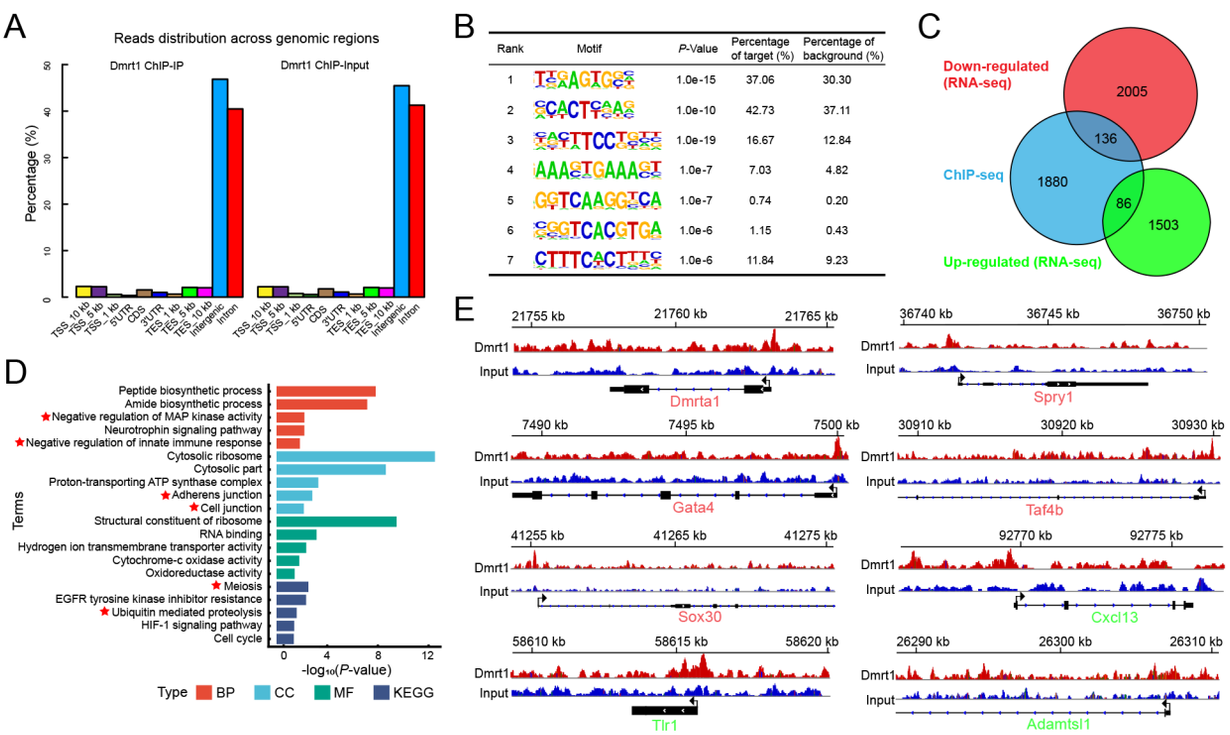

Figure 3 Identification of DMRT1-occupancy sites

A: Location of DMRT1-occupancy peaks relative to nearest annotated gene. B: Sequence motifs enriched at DMRT1-occupancy sites, determined using HOMER. C: Overlapping genes identified by ChIP-seq and RNA-seq analyses. D: Representative biological processes enriched among overlapping genes. Red stars represent important signaling pathways focused on. E: IGV images showing tracks of normalized DMRT1-occupancy tag counts. Representative overlapping genes identified in D are shown. Red, Si-Dmrt1 down-regulated genes bound by DMRT1; green, Si-Dmrt1 up-regulated genes bound by DMRT1. Arrow denotes TSS.

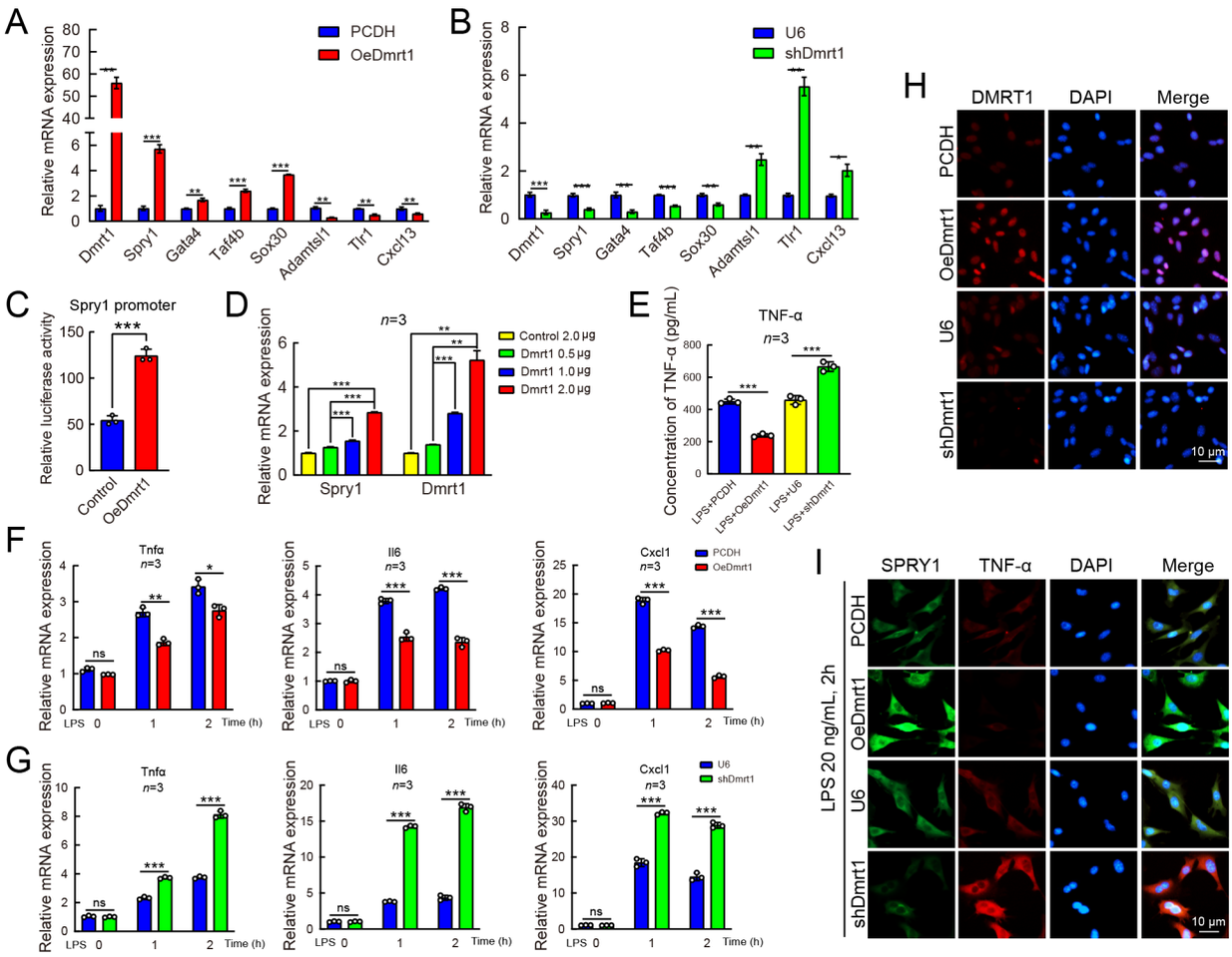

Figure 4 *Dmrt1* directly regulates positive expression of *Spry1*

A: Relative mRNA levels of *Dmrt1*, *Spry1*, *Gata4*, *Taf4b*, *Sox30*, *Adamtsl1*, *Tlr1*, and *Cxcl13* in oeDmrt1 and PCDH TM4 cells (*n*=3). B: Relative mRNA levels of *Dmrt1*, *Spry1*, *Gata4*, *Taf4b*, *Sox30*, *Adamtsl1*, *Tlr1*, and *Cxcl13* in shDmrt1 and U6 TM4 cells (*n*=3). C: Luciferase analysis of constructs harboring *Spry1* promoter ligated upstream of firefly luciferase gene (*Spry1* promoter-Luc). These constructs were transiently cotransfected into TM4 cells with a Dmrt1-expression vector where indicated (*n*=3). D: Relative mRNA levels of *Spry1* in TM4 cells transfected with different doses of *Dmrt1* plasmid as indicated (*n*=3). E: PCDH, OeDmrt1, U6, and shDmrt1 cells were stimulated with LPS for 2 h, with the supernatant then prepared for ELISA of TNF-α (*n*=3). F: qRT-PCR analysis of mRNA levels of *Tnfa*, *Il6*, and *Cxcl1* in PCDH and OeDmrt1 cells stimulated with LPS for indicated time points. G: qRT-PCR analysis of mRNA levels of *Tnfa*, *Il6*, and *Cxcl1* in U6 and shDmrt1 cell lines stimulated with LPS for indicated time points. H: IF analysis of PCDH, OeDmrt1, U6 and shDmrt1 cells stained with antisera against DMRT1, respectively. Cell nuclei were stained with DAPI (blue). Scale bar: 10 μm. I: IF analysis of PCDH, OeDmrt1, U6, and shDmrt1 cells co-stained with antisera against SPRY1 and TNF-α, respectively. Cell nuclei were stained with DAPI (blue). Scale bar: 10 μm. Data are presented as means±*SD* and represent three independent repetitions. ns: Not significant; *: $P<0.05$; **: $P<0.01$; ***: $P<0.001$.

expression increased with *Dmrt1* transfection in a dose-dependent manner (Figure 4D). After LPS treatment for 2 h, the concentration of TNF-α in the supernatant detected by ELISA was reduced in the OeDmrt1 cells and increased in the shDmrt1 cells (Figure 4E). Moreover, ectopic expression of *Dmrt1* attenuated LPS-induced expression of proinflammatory cytokines, including TNF-α, IL-6, and chemokine ligand 1 (CXCL1) (Figure 4F, I). *Dmrt1* KD strengthened LPS-induced expression of these proinflammatory cytokines (Figure 4G, I). Similar results were also obtained by IF staining of DMRT1, SPRY1, and TNF-α in SCs, although SPRY1 was down-regulated (Figure 4H, I). The *Dmrt1* and *Spry1* genes are highly conserved among different species, indicating conserved functional regulation between the two (Supplementary Figure S2A, B). Tissue expression profiles also showed that both were highly expressed in the testes (Supplementary Figure S2C, D). Thus, *Dmrt1* directly regulates the transcriptional expression of *Spry1*, which may affect the immune response of SCs.

Spry1 KD disrupts BTB and immune homeostasis of testis

To explore the function of *Spry1* in the testes, we constructed a mouse model with testicular specific KD of *Spry1* through seminiferous tubule transplantation (Figure 5A). Both qRT-PCR and western blotting confirmed that *Spry1* was successfully knocked down in the Si-Spry1 group (Supplementary Figure S3A, B). Morphology and fecundity of the model mice were tested, with *Spry1* KD testis and epididymis weight both showing a decrease (Figure 5B). Based on histological analysis, the *Spry1* KD testes showed a loose seminiferous epithelium and smaller lumen (Figure 5D), with decreased sperm production (Figure 5C), while no obvious morphological changes were detected in the

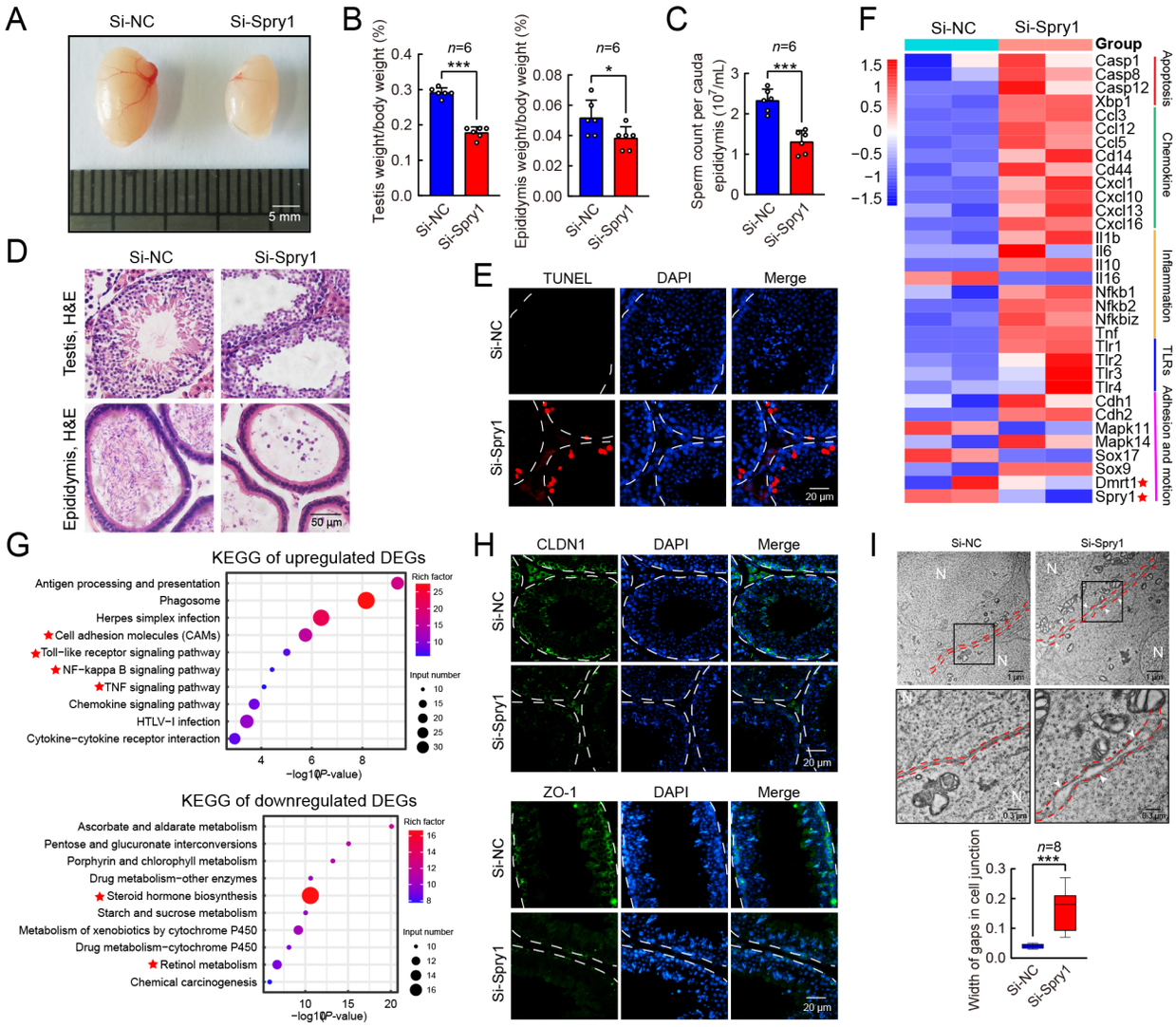

Figure 5 ***Spry1*** **regulates BTB and testicular immune homeostasis**

A: Gross testis morphology shows reduction in testis size in Si-Spry1 group compared with Si-NC group. B: Ratio of testis weight to body weight and epididymis weight to body weight (*n*=6). C: Sperm count per cauda epididymis in Si-NC and Si-Spry1 groups (*n*=6). D: H&E-stained testis (Up) and epididymis (Down) sections from Si-NC and Si-Spry1 groups (*n*=6). Scale bar: 50 μm. E: Cell apoptosis revealed by TUNEL staining of sections from Si-NC and Si-Spry1 testes. Scale bar: 20 μm. F: Heatmap of RNA-seq data showing DEGs in Si-NC and Si-Spry1 testes. G: KEGG analysis of up-regulated DEGs (Up) and down-regulated DEGs (Down) in Si-NC and Si-Spry1 testes. H: IF staining of Claudin 1 (CLDN1) and ZO-1 in Si-NC and Si-Spry1 testes. Cell nuclei were stained with DAPI (blue). Scale bar: 20 μm. CLDN1 and ZO-1 were important components of BTB. I: Transmission electron microscopy visualization of cell junctions in Si-NC and Si-Spry1 testes. Red dashed lines outline cell junctions. White arrows indicate gaps in cell junction. Cell nucleus is labeled by N. Bottom panels are higher magnification images. Scale bar: 1 μm and 0.5 μm. Data are presented as means±*SD* and represent three independent repetitions. *: $P<0.05$; **: $P<0.01$; ***: $P<0.001$.

epididymis (Figure 5D). Sperm motility did not change significantly (Supplementary Figure S3C), but the apoptosis ratio in the seminiferous tubules increased significantly in the Si-Spry1 group (Figure 5E; Supplementary Figure S3H). ELISA detection of serum samples showed that the AsAb level increased significantly, along with the levels of inflammatory factors TNF-α and IL-6 in the Si-Spry1 mice, while GDNF showed a significant decrease (Supplementary Figure S3D).

Transcriptome sequencing was performed to deeply analyze the gene expression pattern in the testis after *Spry1* KD (Supplementary Figure S3E). In total, 1 863 up-regulated genes and 1 914 down-regulated genes were screened, with some representative genes shown in the scatter diagram (Supplementary Figure S3F). The heatmap showed the expression of marker genes in different pathways (Figure 5F). After *Spry1* KD, the expression levels of BTB-related genes were down-regulated, while the expression levels of inflammation-related genes were up-regulated (Figure 5F). GO analysis revealed that the down-regulated genes were enriched in biological processes, including protein binding and glucose metabolism, while the up-regulated genes were enriched in immune system process, immune response, peptidase activity, and innate immune response (Supplementary Figure S3G). KEGG pathway analysis also showed that the down-regulated genes were enriched in steroid hormone biosynthesis, aldosterone synthesis and secretion, and amino acid biosynthesis (Figure 5G), while the up-regulated genes were enriched in cell adhesion molecules and TLR, NF-κB, and TNF signaling pathways (Figure 5G). We detected changes in NF-κB-related genes such as *Tnfα*,

Il1β, *Tlr1*, *Cxcl1*, and *Cxcl10* by qRT-PCR, consistent with the RNA-seq results (Supplementary Figure S3I). IF staining of Si-Spry1 testes revealed that the expression of BTB structural proteins CLDN1 and ZO-1 decreased significantly (Figure 5H). The destruction of the testis and BTB caused by inflammation is an important pathogenic mechanism of testicular autoimmune response, as the BTB can prevent recognition of sperm antigens, which is critical for the maintenance of the testicular immune microenvironment (Wu et al., 2019). These data strongly indicate damage to the testis BTB structure and immune shielding function due to *Spry1* KD. We further used transmission electron microscopy to analyze the ultrastructure of the testicular spermatogenic epithelium. The tight junction structure between SCs in *Spry1* KD testes became looser, and the gap became larger (Figure 5I). These data suggest that *Spry1*, a target gene downstream of *Dmrt1*, is critical for the regulation of testicular BTB integrity and immune homeostasis.

DMRT1-SPRY1-NF-κB regulatory circuit decreases immune response

To further explore how *Dmrt1* and *Spry1* regulates the inflammatory response, we performed joint analysis of the RNA-seq results of the Si-Dmrt1 and Si-Spry1 testes, which revealed 109 co-down-regulated genes and 272 co-up-regulated genes (Figure 6A). KEGG analysis further identified that the co-down-regulated genes were enriched in cortisol synthesis and secretion and steroid hormone biosynthesis, while the co-up-regulated genes were enriched in cell adhesion molecules and the NF-κB and TNF signaling pathways (Figure 6A). The same results were obtained from GO analysis (Supplementary Figure S4A). The expression of representative co-regulatory genes is shown in a heatmap (Figure 6B). Metabolism-related genes *Cyp21a1*, *Cyp17a1*, and *Col17a1* were significantly down-regulated, while NF-κB- and apoptosis-related genes *Nfkbie*, *Ikbke*, *Fas*, *Il1β*, and *Cxcl1* were significantly up-regulated (Figure 6B). Normal SCs were treated with 20 ng/mL LPS for different times and

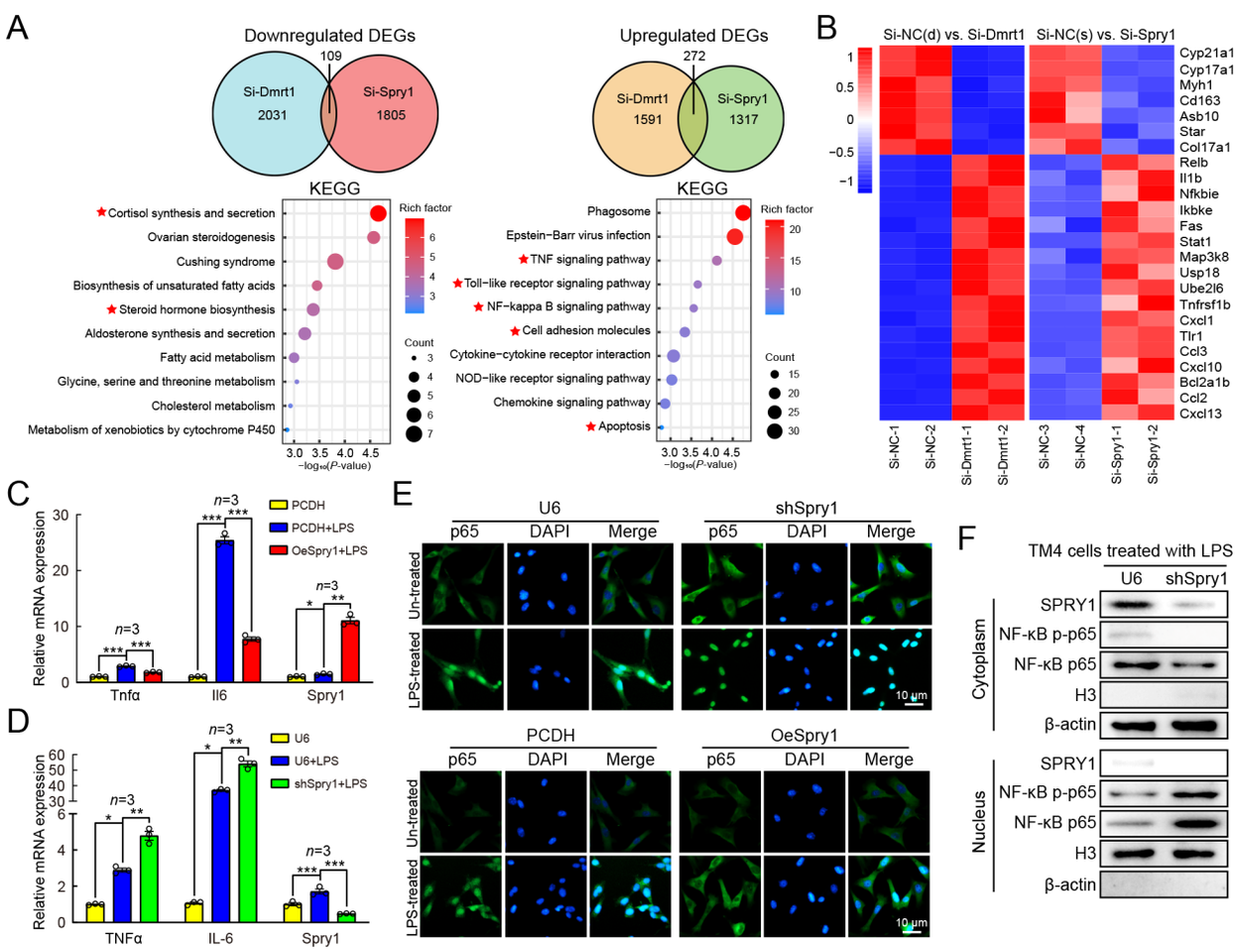

Figure 6 *Spry1* inhibits NF-κB signaling pathway to decrease immune response in SCs

A: Venn diagrams showing overlap of up- and down-regulated DEGs between Si-Dmrt1 and Si-Spry1. KEGG enrichment of up- and down-regulated DEGs are shown below. B: Heatmap of genes co-regulated by *Dmrt1* and *Spry1* enriched in NF-κB signaling pathway, TLR signaling pathway, and apoptosis under different treatments obtained from RNA-seq co-analysis. C: Relative mRNA levels of *Tnfα*, *Il6*, and *Spry1* in PCDH and OeSpry1 cells treated with 20 ng/mL LPS for 2 h (*n*=3). Data were normalized to mRNA levels of respective inflammatory factors in PCDH group without LPS challenge. D: Relative mRNA levels of *Tnfα*, *Il6*, and *Spry1* in U6 and shSpry1 cells treated with 20 ng/mL LPS for 2 h (*n*=3). Data were normalized to mRNA levels of respective inflammatory factors in U6 group without LPS challenge. E: IF analysis of U6, shSpry1, PCDH, and OeSpry1 cells treated with or without LPS for 2 h and stained with antisera against p65, respectively. Cell nuclei were stained with DAPI (blue). Scale bar: 10 μm. F: Western blot analysis of expression levels of SPRY1, p-p65, p65, H3, and β-actin in stably transfected TM4 cells with treatments as indicated. Data are presented as means±*SD* and represent three independent repetitions. *: $P<0.05$; **: $P<0.01$; ***: $P<0.001$.

quantitative detection results showed that *Tnfα* reached the highest value at 1 h and *Spry1* reached the highest value at 2 h, and then began to decline (Supplementary Figure S4B). Cell lines overexpressing *Spry1* (OeSpry1) and short hairpin RNA (shRNA) interfering with *Spry1* (shSpry1) were constructed (Supplementary Figures S2F, S4C). Overexpression of *Spry1* significantly inhibited the expression of *Tnfα* and *Il6* stimulated by LPS (Figure 6C), while inhibition of *Spry1* significantly increased the expression of *Tnfα* and *Il6* induced by LPS (Figure 6D). The expression levels of fibroblast markers *Vim*, *Nfe2l2*, and *Snail1* were up-regulated, while the expression levels of cell adhesion genes *Sox9*, *Tjp1*, *ZO1*, and *Occludin* were down-regulated in the shSpry1 cells (Supplementary Figure S4D). The expression of *Dmrt1* in the shSpry1 cells did not change significantly, but inflammatory factor expression was up-regulated (Supplementary Figure S4E). IF analysis showed that interfering with *Spry1* increased the p65 level significantly, together with a significant increase in nuclear p65 (Figure 6E). In contrast, overexpression of Spry1 resulted in a significant reduction in nuclear p65 (Figure 6E). Nucleocytoplasmic separation showed that *Spry1* KD significantly increased the nuclear translocation of p-p65 activated by LPS (Figure 6F). These findings indicate that the *Dmrt1-Spry1* axis may inhibit the immune response of SCs by controlling NF-κB activation.

Spry1 regulates immunoreaction through interacting with NF-κB

To further explore how SPRY1, the inhibitory protein for RTK signaling, interacts with the NF-κB pathway, we first examined the associations between SPRY1 and key components of the NF-κB pathway in SCs. Results showed that SPRY1 coimmunoprecipitated endogenous NF-κB1 in living SCs (Figure 7A). SPRY1 and NF-κB1 were then immunoprecipitated with antibodies and magnetic beads, followed by mass spectrometry. Results showed that SPRY1 had 476 interacting proteins and NF-κB1 had 1 767 interacting proteins, with 415 proteins overlapping both samples

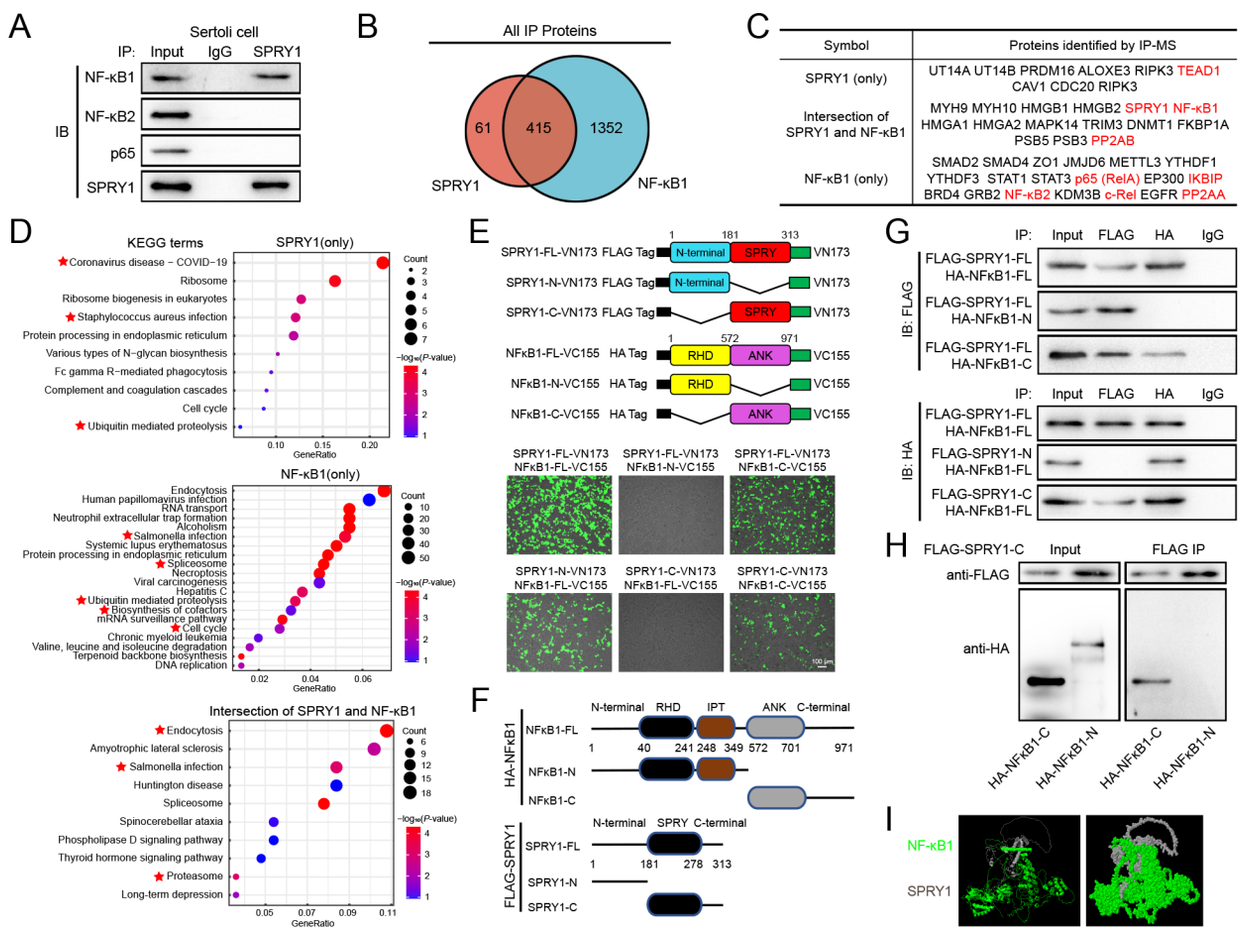

Figure 7 SPRY1 prevents NF-κB nuclear translocation by binding to ANK domain

A: Total lysates were extracted from normal SCs for Co-IP experiments. Equal number of proteins was immunoprecipitated separately with IgG or anti-SPRY1 antibodies. Western blots show expression of NF-κB1, NF-κB2, and p65 with specific antibodies. B: Venn diagrams showing overlap of SPRY1- and NF-κB1-associated proteins determined by mass spectrometry. C: Table lists representative proteins in each section as shown in A. D: KEGG enrichment of SPRY1-associated, NF-κB-associated, SPRY1 and NF-κB co-binding proteins. E: Model for pBiFC-VN173-SPRY1 and pBiFC-VC155-NFκB1 vectors and different domain variants. Two different fusion protein vectors were transfected into HEK293T cells, and green fluorescence expression was observed after 48 h. Stronger green fluorescence indicates that the two proteins bind to each other. F: Indicated truncates of SPRY1 and NF-κB1 were constructed according to functional domains, respectively. G, H: HA-tagged NF-κB mutants with deleted fragments were co-expressed with FLAG-SPRY1 mutants in HEK293T cells. Lysates were immunoprecipitated with anti-FLAG or anti-HA antibodies, and immunoprecipitated protein complex was examined. I: Bioinformatics model for predicting interactions between SPRY1 and NF-κB1 proteins.

(Figure 7B). Thus, the proteins interacting with SPRY1 and NF-κB1 were shown to be co-binding proteins (Figure 7C). KEGG pathway analysis of these groups of interacting proteins showed that the proteins interacting with SPRY1 alone were mainly enriched in *Staphylococcus aureus* infection and coronavirus disease-COVID-19, while the proteins interacting with NF-κB alone were mainly enriched in *Salmonella* infection, cell cycle, ubiquitin-mediated proteolysis, and other pathways. Proteins that interacted with both SPRY1 and NF-κB1 were mainly enriched in endocytosis, *Salmonella* infection, spliceosome, thyroid hormone signaling pathway, and other pathways (Figure 7D). To further explore the domains of the SPRY1 and NF-κB1 interactions, vectors of the SPRY1 and NF-κB1 variants were constructed. SPRY1 and NF-κB1 were divided into two parts, i.e., C- and N-terminal domains (Figure 7E). SPRY1 contained a SPRY domain at the C terminus, while NFKB1 contained an Rel homology domain (RHD), immunoglobulin-plexin-transcription (IPT) domain, and Ankyrin (ANK) domain (Figure 7E). The bimolecular fluorescence complementarity (BiFC) results showed that SPRY1 interacted with NF-κB1 and NF-κB-C terminus to emit green fluorescence, NF-κB interacted with SPRY1 and SPRY1-C terminus to emit green fluorescence, and SPRY1-C and NF-κB-C terminal domains interacted to emit green fluorescence (Figure 7E). Co-IP results further confirmed that the interaction between SPRY1 and NF-κB1 was through the SPRY domain in the C-terminal region of SPRY1 and ANK domain of NF-κB1 (Figure 7F, H). Bioinformatics software predicted the three-dimensional structure of the interaction between SPRY1 and NF-κB1 (Figure 7I). These findings suggested that SPRY1 and NF-κB1 physically interact with each other.

A schematic of the anti-inflammatory effects of *Dmrt1* on SC immune response via the *Spry1* and NF-κB pathways is provided in Figure 8. In brief, *Dmrt1* is expressed in the SCs and SSCs of the testes. LPS or MUV infection in the testes induces acute inflammatory responses, as evidenced by morphological injury, increased cell apoptosis, and aberrant production of inflammatory factors such as TNF-α, IL-6, and CXCL10. Activation of *Spry1* by *Dmrt1* effectively alleviates LPS-induced inflammation in the testes and TM4 cells primarily through combined NF-κB signaling-dependent mechanisms. The SPRY1 protein binds to the ANK domain of NF-κB1 to inhibit NF-κB activation, reduce p-p65 entry into the nucleus, and reduce the cascade reaction of intracellular inflammation to protect the BTB structure of supporting cells and maintain immune homeostasis of the testicular spermatogenic environment. Sustained high expression of *Dmrt1* and *Spry1* in testicular SCs is essential for male reproduction.

DISCUSSION

In mammals, *Dmrt1* plays a crucial role in determination of male sex, maintenance of mitosis and meiosis balance in SSCs, and regulation of male reproductive stem cell pluripotency (Krentz et al., 2009, 2013; Taguchi et al., 2021). *Dmrt1* widely exists in vertebrates and invertebrates and is highly conserved in different species. *Dmrt1* expression persists throughout testicular development, especially in SCs and undifferentiated SSCs (Lei et al., 2007). Studies have shown that *Dmrt1* KO leads to the inability to form testes in fetal mice or to transdifferentiate SCs into granulosa cells in postnatal male mice (Matson et al., 2011; Minkina et al., 2014). In the current study, we explored the role of *Dmrt1* by KD rather than knockout (KO), because *Dmrt1* KO leads to the loss of testicular function. Unlike previous studies, we constructed a testis-specific *Dmrt1* KD model by transfecting shRNA into seminiferous tubules. Due to the almost exclusive high expression of *Dmrt1* in SCs, as well as the existence of the BTB, we specifically knocked down *Dmrt1* in the SCs of the testes of mice. Results showed that mice with testis-

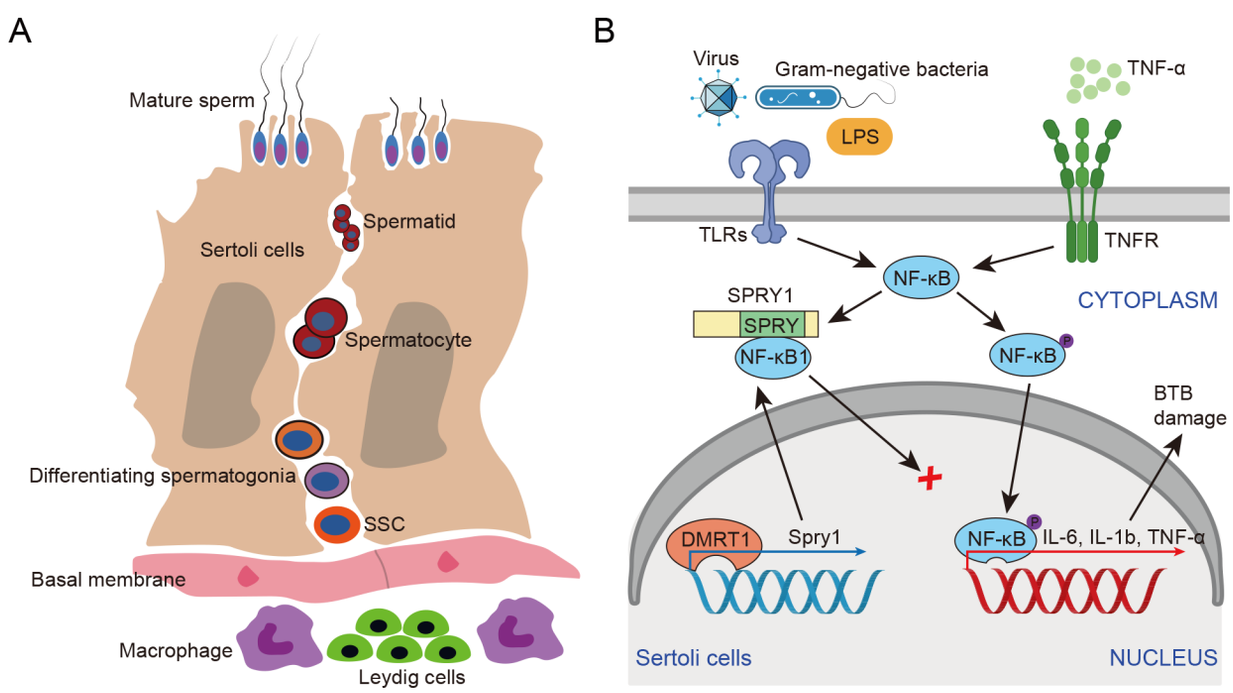

Figure 8 Role of DMRT1 and SPRY1 in SCs

Proposed model for *Dmrt1* activation of downstream *Spry1* signaling pathway to regulate immunoreaction in SCs. Loss of *Dmrt1* or *Spry1* in SCs mediates NF-κB activation in SC growth, leading to changes in immune microenvironment.

specific *Dmrt1* KD presented with dyszoospermia and decreased sperm motility, consistent with previous findings (Zhang et al., 2016). In addition, *Dmrt1* KD resulted in an increase in multinucleated giant cells in spermatogenic epithelium, apoptosis, BTB permeability, blood AsAb, and intratesticular inflammatory factors. Transcriptome sequencing showed that the expression levels of germ cells and meiosis-related genes was down-regulated, while the expression of inflammation-related genes was up-regulated. These *in vivo* results indicated that the reproductive immune microenvironment of mouse testes changed after *Dmrt1* KD. Furthermore, ChIP-seq and RNA-seq analyses revealed that *Dmrt1* positively regulated the expression levels of *Dmrta1*, *Spry1*, *Gata4*, *Taf4b*, *Sox30*, and other genes, and negatively regulated the expression levels of *Cxcl13*, *Tlr1*, *Adamtsl1*, and other genes, relatively consistent with previous reports (Lindeman et al., 2021; Tan et al., 2021). These results strongly indicate that *Dmrt1* is involved in the maintenance of the testicular reproductive immune microenvironment and plays an important negative regulatory role in the process of orchitis.

The mammalian testis creates a unique immune environment important for spermatogenesis. The testicular immune microenvironment consists of common immune cells and other cells involved in testicular immunity. The former includes testicular macrophages, T cells, dendritic cells (DC), and hypertrophied cells, while the latter includes Leydig cells and SCs (Defalco et al., 2015; Fang et al., 2021). SCs are involved in BTB formation and play a central role in establishing and maintaining the testicular immune privilege. Due to the tight connection between SCs in seminiferous tubules, germ cells are protected from pathogens to carry out normal spermatogenesis (Chi et al., 2021; Matson et al., 2010). SC maintenance requires the continuous high expression of *Dmrt1*, highlighting the importance of *Dmrt1* in the regulation of the testicular microenvironment (Raverdeau et al., 2012). SCs also regulate the immune response (Doyle et al., 2012; Winnall et al., 2011). In addition, Leydig cells are very important in the regulation of spermatogenesis and can secrete many cytokines (Shen et al., 2021). The regulatory relationship between Leydig cells and SCs warrants further research.

The innate immune response is primarily triggered by TLRs against invasive pathogens (De Nardo, 2015). SCs contain Tlr2–Tlr6, which initiate the innate immune response and induce the expression of major proinflammatory cytokines (Zhang et al., 2013). In response to MUV infection, SCs produce higher levels of TNF-α and IL-6 than Leydig cells (Wu et al., 2019). Under physiological conditions, low levels of proinflammatory cytokines are essential for normal spermatogenesis. However, these cytokines are highly expressed under inflammatory conditions, inducing testicular dysfunction and male germ cell apoptosis (Chen et al., 2016). TLRs activate the myeloid differentiation protein 88 (MyD88)-dependent pathway, which stimulates NF-κB and mitogen activated protein kinases (MAPKs) and activates a variety of proinflammatory cytokines, including TNF-α, IL-6, and IL-1β. Here, our *in vitro* and *in vivo* studies showed that: 1) LPS-induced inflammatory response activated the NF-κB signaling pathway to produce excess TNF-α and IL-6, resulting in the destruction of the BTB; and 2) Increased inflammatory factors led to a decrease in the expression of tight junction proteins ZO-1 and CLDN1, consistent with previous studies (Jia et al., 2017; Thomas et al., 2020). Our current results showed that *Dmrt1* can inhibit excessive inflammatory response by regulating *Spry1* expression, and both proteins can inhibit NF-κB activation. Therefore, our study identified a new role of *Dmrt1* in regulating testicular immune homeostasis.

Spry1, a negative regulator of RTK signal transduction, is a member of the Sprouty gene family, recognized by significant sequence homologies, including a conserved cysteine-rich SPRY domain located in the C-terminal region and a short N-terminal amino acid sequence (Cabrita & Christofori, 2008). *Spry1* is involved in the regulation of various diseases, including lung fibrosis, cardiac dysfunction, and cell aging response. Notably, activation of the AMFR-*Spry1* pathway by the chemokine CCL1 has been shown to promote lung fibrosis (Liu et al., 2021), while inhibition of *Spry1* in cardiomyocytes activates the ERK and p38 mitogen-activated protein kinase signaling pathways (Alakoski et al., 2019; Hanafusa et al., 2002). Additionally, studies involving *Spry1* knockout mice have revealed that *Spry1* not only weakens RTK signaling in the thyroid gland but also induces a cell aging response to prevent uncontrolled proliferation (Macià et al., 2014). Moreover, we showed that the highly conserved cysteine-rich C-terminal domain SPRY of SPRY1 binds to the ANK repeat of NF-κB1, thereby inhibiting the activation of NF-κB and preventing excessive inflammatory response in the testis, thus maintaining testicular immune homeostasis (De Oliveira et al., 2016; Shih et al., 2012).

CONCLUSIONS

Our investigation elucidated a crucial function of *Dmrt1* in spermatogenesis and the regulation of testicular immune response via the *Dmrt1*-*Spry1*-NF-κB signaling axis. This finding is of great significance for comprehending the mechanisms underlying testicular immune homeostasis regulation and developing novel therapeutics for male reproductive disorders.

DATA AVAILABILITY

Raw sequencing reads were deposited in the Gene Expression Omnibus (GEO) database (https://www.ncbi.nlm.nih.gov/geo, GSE212664, GSE212665, GSE212667), GSA database (https://www.cncb.ac.cn/, PRJCA015052), and Science Data Bank database (https://www.scidb.cn/en, DOI: 10.57760/sciencedb.07482). Mass spectrometry proteomics data were deposited in the ProteomeXchange Consortium (http://proteomecentral.proteomexchange.org) via the PRIDE partner repository with dataset identifier PXD036516.

SUPPLEMENTARY DATA

Supplementary data to this article can be found online.

COMPETING INTERESTS

The authors declare that they have no competing interests.

AUTHORS' CONTRIBUTIONS

J.L.H. and M.F.Z. designed the research and wrote the manuscript. M.F.Z. performed most of the experiments. S.C.W., W.B.C., D.H.Y., B.L.L., A.A., X.M.D., Y.X.L., W.P.W., and X.C.Y. performed the animal experiments. W.Q.L., Y.D.W., N.L., S.P., X.L.L., G.P.L., and J.L.H. analyzed high-throughput sequencing data. All authors read and approved the final version of the manuscript.

ACKNOWLEDGMENTS

We appreciate Prof. Xiao-Ming Liu, Prof. Yong Tang, and Dr Qi-Jing Lei for their constructive comments and careful revision of this manuscript.

REFERENCES

Alakoski T, Ulvila J, Yrjölä R, et al. 2019. Inhibition of cardiomyocyte Sprouty1 protects from cardiac ischemia-reperfusion injury. *Basic Research in Cardiology*, **114**(2): 7.

Brinster RL, Avarbock MR. 1994. Germline transmission of donor haplotype following spermatogonial transplantation. *Proceedings of the National Academy of Sciences of the United States of America*, **91**(24): 11303−11307.

Cabrita MA, Christofori G. 2008. Sprouty proteins, masterminds of receptor tyrosine kinase signaling. *Angiogenesis*, **11**(1): 53−62.

Chen QY, Deng TT, Han DS. 2016. Testicular immunoregulation and spermatogenesis. *Seminars in Cell & Developmental Biology*, **59**: 157−165.

Chi XC, Luo WW, Song JG, et al. 2021. Kindlin-2 in Sertoli cells is essential for testis development and male fertility in mice. *Cell Death & Disease*, **12**(6): 604.

De Nardo D. 2015. Toll-like receptors: activation, signalling and transcriptional modulation. *Cytokine*, **74**(2): 181−189.

De Oliveira KAP, Kaergel E, Heinig M, et al. 2016. A roadmap of constitutive NF-κB activity in Hodgkin lymphoma: dominant roles of p50 and p52 revealed by genome-wide analyses. *Genome Medicine*, **8**(1): 28.

Defalco T, Potter SJ, Williams AV, et al. 2015. Macrophages contribute to the spermatogonial niche in the adult testis. *Cell Reports*, **12**(7): 1107−1119.

Dobin A, Davis CA, Schlesinger F, et al. 2013. STAR: ultrafast universal RNA-seq aligner. *Bioinformatics*, **29**(1): 15−21.

Doyle TJ, Kaur G, Putrevu SM, et al. 2012. Immunoprotective properties of primary Sertoli cells in mice: potential functional pathways that confer immune privilege. *Biology of Reproduction*, **86**(1): 1−14.

Du ZY, Xu SS, Hu SX, et al. 2018. Melatonin attenuates detrimental effects of diabetes on the niche of mouse spermatogonial stem cells by maintaining Leydig cells. *Cell Death & Disease*, **9**(10): 968.

Fang YW, Su YF, Xu J, et al. 2021. Varicocele-mediated male infertility: from the perspective of testicular immunity and inflammation. *Frontiers in Immunology*, **12**: 729539.

Feng CW, Burnet G, Spiller CM, et al. 2021. Identification of regulatory elements required for *Stra8* expression in fetal ovarian germ cells of the mouse. *Development*, **148**(5): dev194977.

Fijak M, Pilatz A, Hedger MP, et al. 2018. Infectious, inflammatory and 'autoimmune' male factor infertility: how do rodent models inform clinical practice?. *Human Reproduction Update*, **24**(4): 416−441.

Goodyear S, Brinster R. 2017. Spermatogonial stem cell transplantation to the testis. *Cold Spring Harbor Protocols*, **2017**(4): pdb.prot094235.

Govero J, Esakky P, Scheaffer SM, et al. 2016. Zika virus infection damages the testes in mice. *Nature*, **540**(7633): 438−442.

Hanafusa H, Torii S, Yasunaga T, et al. 2002. Sprouty1 and Sprouty2 provide a control mechanism for the Ras/MAPK signalling pathway. *Nature Cell Biology*, **4**(11): 850−858.

Hancock ML, Meyer RC, Mistry M, et al. 2019. Insulin receptor associates with promoters genome-wide and regulates gene expression. *Cell*, **177**(3): 722−736.e22.

Hou PP, Jia PH, Yang KX, et al. 2021. An unconventional role of an ASB family protein in NF-κB activation and inflammatory response during microbial infection and colitis. *Proceedings of the National Academy of Sciences of the United States of America*, **118**(3): e2015416118.

Hui LX, Nie YW, Li SH, et al. 2020. Matrix metalloproteinase 9 facilitates Zika virus invasion of the testis by modulating the integrity of the blood-testis barrier. *PLoS Pathogens*, **16**(4): e1008509.

Ioannidis J, Taylor G, Zhao DB, et al. 2021. Primary sex determination in birds depends on DMRT1 dosage, but gonadal sex does not determine adult secondary sex characteristics. *Proceedings of the National Academy of Sciences of the United States of America*, **118**(10): e2020909118.

Jia XY, Xu Y, Wu WX, et al. 2017. Aroclor1254 disrupts the blood-testis barrier by promoting endocytosis and degradation of junction proteins via p38 MAPK pathway. *Cell Death & Disease*, **8**(5): e2823.

Kanatsu-Shinohara M, Morimoto H, Shinohara T. 2016. Fertility of male germline stem cells following spermatogonial transplantation in infertile mouse models. *Biology of Reproduction*, **94**(5): 112.

Kanatsu-Shinohara M, Ogonuki N, Inoue K, et al. 2003. Restoration of fertility in infertile mice by transplantation of cryopreserved male germline stem cells. *Human Reproduction*, **18**(12): 2660−2667.

Kim D, Pertea G, Trapnell C, et al. 2013. TopHat2: accurate alignment of transcriptomes in the presence of insertions, deletions and gene fusions. *Genome Biology*, **14**(4): R36.

Koledova Z, Zhang XH, Streuli C, et al. 2016. SPRY1 regulates mammary epithelial morphogenesis by modulating EGFR-dependent stromal paracrine signaling and ECM remodeling. *Proceedings of the National Academy of Sciences of the United States of America*, **113**(39): E5731−E5740.

Krentz AD, Murphy MW, Kim S, et al. 2009. The DM domain protein DMRT1 is a dose-sensitive regulator of fetal germ cell proliferation and pluripotency. *Proceedings of the National Academy of Sciences of the United States of America*, **106**(52): 22323−22328.

Krentz AD, Murphy MW, Zhang T, et al. 2013. Interaction between DMRT1 function and genetic background modulates signaling and pluripotency to control tumor susceptibility in the fetal germ line. *Developmental Biology*, **377**(1): 67−78.

Lei N, Hornbaker KI, Rice DA, et al. 2007. Sex-specific differences in mouse DMRT1 expression are both cell type- and stage-dependent during gonad development. *Biology of Reproduction*, **77**(3): 466−475.

Lei QJ, Pan Q, Li N, et al. 2019. H19 regulates the proliferation of bovine male germline stem cells via IGF-1 signaling pathway. *Journal of Cellular Physiology*, **234**(1): 915−926.

Li Y, Su YF, Zhou T, et al. 2019. Activation of the NLRP3 Inflammasome Pathway by Prokineticin 2 in Testicular Macrophages of Uropathogenic *Escherichia coli*- Induced Orchitis. *Frontiers in Immunology*, **10**: 1872.

Liao Y, Smyth GK, Shi W. 2014. featureCounts: an efficient general purpose program for assigning sequence reads to genomic features. *Bioinformatics*, **30**(7): 923−930.

Lie PP, Cheng CY, Mruk DD. 2011. Interleukin-1alpha is a regulator of the blood-testis barrier. *FASEB Journal:Official Publication of the Federation of American Societies For Experimental Biology*, **25**(4): 1244−1253.

Lindeman RE, Murphy MW, Agrimson KS, et al. 2021. The conserved sex regulator DMRT1 recruits SOX9 in sexual cell fate reprogramming. *Nucleic Acids Research*, **49**(11): 6144−6164.

Liu SS, Liu C, Lv XX, et al. 2021. The chemokine CCL1 triggers an AMFR-SPRY1 pathway that promotes differentiation of lung fibroblasts into myofibroblasts and drives pulmonary fibrosis. *Immunity*, **54**(9): 2042−2056.e8.

Lou RH, Liu WZ, Li RJ, et al. 2021. DeepPhospho accelerates DIA phosphoproteome profiling through in silico library generation. *Nature Communications*, **12**(1): 6685.

Lu YN, Bhushan S, Tchatalbachev S, et al. 2013. Necrosis is the dominant

cell death pathway in uropathogenic *Escherichia coli* elicited epididymo-orchitis and is responsible for damage of rat testis. *PLoS One*, **8**(1): e52919.

Ma WQ, Li SH, Ma SQ, et al. 2016. Zika virus causes testis damage and leads to male infertility in mice. *Cell*, **167**(6): 1511−1524.e10.

Macià A, Vaquero M, Gou-Fàbregas M, et al. 2014. Sprouty1 induces a senescence-associated secretory phenotype by regulating NFκB activity: implications for tumorigenesis. *Cell Death & Differentiation*, **21**(2): 333−343.

Malolina EA, Kulibin AY, Naumenko VA, et al. 2014. Herpes simplex virus inoculation in murine rete testis results in irreversible testicular damage. *International Journal of Experimental Pathology*, **95**(2): 120−130.

Matson CK, Murphy MW, Griswold MD, et al. 2010. The mammalian doublesex homolog DMRT1 is a transcriptional gatekeeper that controls the mitosis versus meiosis decision in male germ cells. *Developmental Cell*, **19**(4): 612−624.

Matson CK, Murphy MW, Sarver AL, et al. 2011. DMRT1 prevents female reprogramming in the postnatal mammalian testis. *Nature*, **476**(7358): 101−104.

Mawaribuchi S, Musashijima M, Wada M, et al. 2017. Molecular evolution of two distinct dmrt1 promoters for germ and somatic cells in vertebrate gonads. *Molecular Biology and Evolution*, **34**(3): 724−733.

Mazaud-Guittot S, Meugnier E, Pesenti S, et al. 2010. Claudin 11 deficiency in mice results in loss of the Sertoli cell epithelial phenotype in the testis. *Biology of Reproduction*, **82**(1): 202−213.

Meinhardt A. 2017. A new threat on the horizon - Zika virus and male fertility. *Nature Reviews Urology*, **14**(3): 135−136.

Meng J, Greenlee AR, Taub CJ, et al. 2011. Sertoli cell-specific deletion of the androgen receptor compromises testicular immune privilege in mice. *Biology of Reproduction*, **85**(2): 254−260.

Minkina A, Matson CK, Lindeman RE, et al. 2014. DMRT1 protects male gonadal cells from retinoid-dependent sexual transdifferentiation. *Developmental Cell*, **29**(5): 511−520.

Mruk DD, Cheng CY. 2015. The mammalian blood-testis barrier: its biology and regulation. *Endocrine Reviews*, **36**(5): 564−591.

Ogawa T, Aréchaga JM, Avarbock MR, et al. 1997. Transplantation of testis germinal cells into mouse seminiferous tubules. *The International Journal of Developmental Biology*, **41**(1): 111−122.

Ogita Y, Mawaribuchi S, Nakasako K, et al. 2020. Parallel evolution of two *dmrt1*-derived genes, *dmy* and *dm-W*, for vertebrate sex determination. *iScience*, **23**(1): 100757.

Punab M, Poolamets O, Paju P, et al. 2017. Causes of male infertility: a 9-year prospective monocentre study on 1737 patients with reduced total sperm counts. *Human Reproduction*, **32**(1): 18−31.

Purpura LJ, Alukal J, Chong AM, et al. 2022. SARS-CoV-2 RNA shedding in semen and oligozoospermia of patient with severe coronavirus disease 11 weeks after infection. *Emerging Infectious Diseases*, **28**(1): 196−200.

Qin DZ, Cai H, He C, et al. 2021. Melatonin relieves heat-induced spermatocyte apoptosis in mouse testes by inhibition of ATF6 and PERK signaling pathways. *Zoological Research*, **42**(4): 514−524.

Raverdeau M, Gely-Pernot A, Féret B, et al. 2012. Retinoic acid induces Sertoli cell paracrine signals for spermatogonia differentiation but cell autonomously drives spermatocyte meiosis. *Proceedings of the National Academy of Sciences of the United States of America*, **109**(41): 16582−16587.

Rodríguez-Mateo C, Torres B, Gutiérrez G, et al. 2017. Downregulation of Lnc-Spry1 mediates TGF-*β*-induced epithelial-mesenchymal transition by transcriptional and posttranscriptional regulatory mechanisms. *Cell Death & Differentiation*, **24**(5): 785−797.

Shen YC, Shami AN, Moritz L, et al. 2021. TCF21^{+} mesenchymal cells contribute to testis somatic cell development, homeostasis, and regeneration in mice. *Nature Communications*, **12**(1): 3876.

Shih VFS, Davis-Turak J, Macal M, et al. 2012. Control of RelB during dendritic cell activation integrates canonical and noncanonical NF-κB pathways. *Nature Immunology*, **13**(12): 1162−1170.

Taguchi J, Shibata H, Kabata M, et al. 2021. DMRT1-mediated reprogramming drives development of cancer resembling human germ cell tumors with features of totipotency. *Nature Communications*, **12**(1): 5041.

Takashima S, Hirose M, Ogonuki N, et al. 2013. Regulation of pluripotency in male germline stem cells by Dmrt1. *Genes & Development*, **27**(18): 1949−1958.

Tan K, Song HW, Wilkinson MF. 2021. RHOX10 drives mouse spermatogonial stem cell establishment through a transcription factor signaling cascade. *Cell Reports*, **36**(3): 109423.

Thomas PA, Schafler ED, Ruff SE, et al. 2020. UXT in Sertoli cells is required for blood-testis barrier integrity. *Biology of Reproduction*, **103**(4): 880−891.

Thorvaldsdóttir H, Robinson JT, Mesirov JP. 2013. Integrative genomics viewer (IGV): high-performance genomics data visualization and exploration. *Briefings in Bioinformatics*, **14**(2): 178−192.

Vijay K. 2018. Toll-like receptors in immunity and inflammatory diseases: past, present, and future. *International Immunopharmacology*, **59**: 391−412.

Virtanen HE, Jørgensen N, Toppari J. 2017. Semen quality in the 21st century. *Nature Reviews Urology*, **14**(2): 120−130.

Wang L, Sun F, Wan ZY, et al. 2022. Transposon-induced epigenetic silencing in the X chromosome as a novel form of *dmrt1* expression regulation during sex determination in the fighting fish. *BMC Biology*, **20**(1): 5.

Wang MW, Yang Z, Chen X, et al. 2021. Activation of PTH1R alleviates epididymitis and orchitis through Gq and β-arrestin-1 pathways. *Proceedings of the National Academy of Sciences of the United States of America*, **118**(45): e2107363118.

Wang WB, Li G, De W, et al. 2018. Zika virus infection induces host inflammatory responses by facilitating NLRP3 inflammasome assembly and interleukin-1β secretion. *Nature Communications*, **9**(1): 106.

Wang ZP, Xu XJ. 2020. scRNA-seq profiling of human testes reveals the presence of the ACE2 receptor, a target for SARS-CoV-2 infection in spermatogonia, leydig and sertoli cells. *Cells*, **9**(4): 920.

Wei YD, Cai SF, Ma FL, et al. 2018. Double sex and mab-3 related transcription factor 1 regulates differentiation and proliferation in dairy goat male germline stem cells. *Journal of Cellular Physiology*, **233**(3): 2537−2548.

Wei YD, Du XM, Yang DH, et al. 2021. Dmrt1 regulates the immune response by repressing the TLR4 signaling pathway in goat male germline stem cells. *Zoological Research*, **42**(1): 14−27.

Wiles TJ, Kulesus RR, Mulvey MA. 2008. Origins and virulence mechanisms of uropathogenic *Escherichia coli*. *Experimental and Molecular Pathology*, **85**(1): 11–19.

Winnall WR, Muir JA, Hedger MP. 2011. Differential responses of epithelial Sertoli cells of the rat testis to Toll-like receptor 2 and 4 ligands: implications for studies of testicular inflammation using bacterial lipopolysaccharides. *Innate Immunity*, **17**(2): 123−136.

Wu H, Jiang X, Gao YX, et al. 2019. Mumps virus infection disrupts blood-

testis barrier through the induction of TNF-α in Sertoli cells. *FASEB Journal:Official Publication of the Federation of American Societies For Experimental Biology*, **33**(11): 12528−12540.

Wu H, Wang F, Tang DD, et al. 2021a. Mumps orchitis: clinical aspects and mechanisms. *Frontiers in Immunology*, **12**: 582946.

Wu JM, Mao XZ, Cai T, et al. 2006. KOBAS server: a web-based platform for automated annotation and pathway identification. *Nucleic Acids Research*, **34**(S2): W720−W724.

Wu XL, Zhu ZS, Xiao X, et al. 2021b. *LIN28A* inhibits *DUSP* family phosphatases and activates MAPK signaling pathway to maintain pluripotency in porcine induced pluripotent stem cells. *Zoological Research*, **42**(3): 377−388.

Xia WL, Wong EWP, Mruk DD, et al. 2009. TGF-β3 and TNFα perturb blood-testis barrier (BTB) dynamics by accelerating the clathrin-mediated endocytosis of integral membrane proteins: a new concept of BTB regulation during spermatogenesis. *Developmental Biology*, **327**(1): 48−61.

Yang XC, Wu XL, Li WH, et al. 2022. *OCT6* inhibits differentiation of porcine-induced pluripotent stem cells through MAPK and PI3K signaling regulation. *Zoological Research*, **43**(6): 911−922.

Yin HQ, Kang ZL, Zhang YW, et al. 2021. HDAC3 controls male fertility through enzyme-independent transcriptional regulation at the meiotic exit of spermatogenesis. *Nucleic Acids Research*, **49**(9): 5106−5123.

Yu XW, Li TT, Du XM, et al. 2021. Single-cell RNA sequencing reveals atlas of dairy goat testis cells. *Zoological Research*, **42**(4): 401−405.

Zhang JQ, Guo JX, Wu XJ, et al. 2022. Optimization of sgRNA expression strategy to generate multiplex gene-edited pigs. *Zoological Research*, **43**(6): 1005−1008.

Zhang MF, Li N, Liu WQ, et al. 2021. *Eif2s3y* promotes the proliferation of spermatogonial stem cells by activating ERK signaling. *Stem Cells International*, **2021**: 6668658.

Zhang T, Oatley J, Bardwell VJ, et al. 2016. DMRT1 is required for mouse spermatogonial stem cell maintenance and replenishment. *PLoS Genetics*, **12**(9): e1006293.

Zhang XY, Wang T, Deng TT, et al. 2013. Damaged spermatogenic cells induce inflammatory gene expression in mouse Sertoli cells through the activation of Toll-like receptors 2 and 4. *Molecular and Cellular Endocrinology*, **365**(2): 162−173.

Zhu ZS, Wu XL, Li Q, et al. 2021. Histone demethylase complexes KDM3A and KDM3B cooperate with OCT4/SOX2 to define a pluripotency gene regulatory network. *FASEB Journal:Official Publication of the Federation of American Societies for Experimental Biology*, **35**(6): e21664.